



MASS TRANSFER EFFICIENCY FOR CO₂ CAPTURE USING SODA SOLUTIONS

Lappeenranta–Lahti University of Technology LUT

Master's Programme in Chemical Engineering and Water Treatment, Master's Thesis
2021

Mohankumar Narayanasamy

Examiners: Professor Tuomas Koiranen D.Sc. (Tech)

Supervisors: Kristian Melin D.Sc (Tech)

Tuula Kajolinna M.Eng

ABSTRACT

Lappeenranta–Lahti University of Technology LUT

LUT School of Engineering Science

Chemical Engineering and Water Treatment

Mohankumar Narayanasamy

Mass Transfer Efficiency for CO₂ Capture Using Soda Solutions

Master's Thesis

2021

85 Pages, 49 Figures, 12 Tables

Examiners: Professor Tuomas Koiranen, D.Sc. (Tech)

Supervisor: Kristian Melin D.Sc. (Tech)

Tuula Kajolinna M.Eng.

Keywords: E-fuels, Power to X, BECCU, Green electrification, carbonate processes, mass transfer efficiency, High-Speed camera.

The global emissions from transportation division and the demand for synthetic fuels to diminish emissions is anticipated a mammoth growth in the upcoming years. To offset the emissions produced in biogenic processes is to capture the maximum CO₂ gas which is produced during the processes and utilizing it in the production of e-fuel, which will boost the efficiency and ameliorates the plan of becoming carbon neutral by 2035 as proposed by Finnish Government's climate policy.

In this thesis various methods for CO₂ capture, methods used to measure mass transfer rates of flue gas, acceleration techniques of mass transfer rates in gas absorption and approaches in optimizing the process will be reviewed. Absorption based post-combustion capture technology developed by VTT (Enhanced soda scrubbing process) were experimented using a high-performance bubble generation device at pilot scale container using synthetic gas mixtures at various experimental setup. Since the absorption rates of gas were unknown more exact measurements were performed to determine the gas absorption rates so that it can be used in future scale up and for more rigorous performance evaluation. The gas bubble images were recorded by high-speed camera which is useful in determining the average bubble size.

Enhanced soda scrubbing process for carbon capture was tested, it is observed that the absorption rate and capacity is higher when compared to water, due to chemical reaction the absorption of the pollutant gas is ten times higher, higher delay time after the bubble producing device was not effective, with vertically mounted bubble producing device promising results were achieved at realistic conditions. Capture efficiency of 90% was achieved at 1 bar pressure without regeneration and an optimal L/G ratio 1.25 was identified which produces best results as trade-off between input energy power and mass transfer rate. Nevertheless further

investigation and experiments are necessary to achieve better results and technoeconomic evaluation of tested technology is needed.

PREFACE AND ACKNOWLEDGEMENTS

This thesis work is conducted as a part of E-Fuels project financed jointly by Business Finland and VTT. The project is mainly led by VTT and it is a collective project between an association formed by several Finnish companies and partners from diverse industries together with worldwide research groups. Primary aim of E-Fuels project is developing cleaner transportation fuel solutions, improving utilization technologies of carbon dioxide in the production of valuable chemical products.

I wish to express my sincere gratitude towards my supervisors Kristian Melin, Tuula Kajolinna, for their valuable guidance and constant supervision as well as for providing necessary information. I am grateful for the trust and responsibility that I was given. I am much thankful to Professor Tuomas Koiranen for his enriching guidance on this thesis and for all the knowledge and expertise he has passed on during my studies. I also thank VTT's Renewable Energy Processes team for providing a conducive atmosphere and giving a good learning experience. I am much thankful to Dmitry Vladimirovich Gradov, Tuomas Sihvonen, Soheil Aghajanian, Pavel Maksimov for their instrumental help in simulation. My sincere thanks to Andrey Saren for recording the images.

I would like to thank my friends for being supportive and encouraging at the tough times. Last but not the least, I am eternally thankful to my parents for their love, patience and kindness towards me.

TABLE OF CONTENTS

ABSTRACT.....	2
PREFACE AND ACKNOWLEDGEMENTS.....	4
SYMBOLS AND ABBREVIATIONS	7
1 INTRODUCTION	10
1.1 Carbon capture, storage and its subsequent impact	11
1.2 E-Fuel Production	12
1.3 BECCU	13
2 OBJECTIVE	13
LITERATURE REVIEW	14
3 REVIEW ON CO ₂ CAPTURE PROCESSES BASED ON CARBONATES	14
3.1 Waste Incinerator- CO ₂ Capture and re-use.....	14
3.2 Vartan Bioenergy Plant- Idea.....	16
3.3 Microencapsulated liquid sorbents for CO ₂ capture	16
3.4 Promoted CO ₂ capture using Bio catalyst.....	17
4 PHENOMENA IN SODA BASED CO ₂ CAPTURE	18
4.1 Chemistry in soda-based CO ₂ capture.....	18
4.2 Chemical Reactions	18
4.3 Gas solubilities by Henry's law	18
4.4 Kinetics of CO ₂ absorption in soda-based solutions	21
5 MASS TRANSFER	21
5.1 Theory of mass transfer.....	21
5.2 Mass Transfer rate.....	22
5.3 Film Theory	22
5.4 Two-Film Theory	23
5.5 Mass transfer coefficients of gases and liquids.....	24
5.6 Enhancement Factor.....	25
6 MEASUREMENT OF MASS TRANSFER IN CO ₂ -CARBONATE SYSTEM	25
6.1 Attempt to measure interfacial area	25
6.2 CO ₂ absorption rates by wetted column and string of disc apparatus	27
7 ENHANCEMENT OF MASS TRANSFER FOR SODA-BASED CO ₂ CAPTURE.....	32
7.1 Bubble size and mass transfer	32
7.2 Improvement of absorption rate by PPGME.....	32
8 MICROBUBBLE GENERATION DEVICES	34
8.1 Venturi type bubble generator.....	34

8.2	Oxygen dissolution by venturi-orifice bubble generator	35
EXPERIMENTAL PART		36
9	DESCRIPTION OF THE CARBON CAPTURE EXPERIMENTS IN THE PILOT UNIT	36
9.1	Data Processing.....	38
9.2	Dissolved oxygen measurements	39
9.3	Results - Mass transfer rate estimation for dissolved oxygen measurement.....	43
9.4	Description of Mass transfer rate estimation from CO ₂ and 8 w-% Na ₂ CO ₃ experiments ...	47
9.5	Results - Mass transfer rate estimation from CO ₂ and 8 w-% Na ₂ CO ₃ experiments	49
9.6	Description of the bubble size measurements	56
9.7	Results – Bubble size measurements	58
9.8	Pumping energy as a trade-off for kLa.....	66
10	EVALUATION OF THE EXPERIMENTS AND LIMITATIONS	67
11	CONCLUSION.....	69
12	FUTURE RESEARCH	71
13	REFERENCES	72

SYMBOLS AND ABBREVIATIONS

Abbreviations

BECCS	Bioenergy with Carbon Capture and Storage
BECCU	Bioenergy with Carbon Capture and Utilization
CCS	Carbon Capture and Storage
CCU	Carbon Capture and Utilization
CFD	Computational Fluid Dynamics
CLR	Continuous Loop Reactor
CR	Capture Rate
CSTR	Continuous Stirred Tank Reactor
DEA	Di ethanol Amine
DO	Dissolved Oxygen
DO	Dissolved Oxygen
GHG	Greenhouse Gas
GtCO ₂	Giga ton of Carbon dioxide
HPC	Hot Potassium Carbonate
HSCP	Hydrated Sodium Carbonate Powders
IEA	International Energy Agency
IPCC	Intergovernmental Panel on Climate change
IVCAP	Integrated Vacuum Carbonate Absorption Process
MEA	Mono ethanolamine
MECS	Microencapsulated Carbon Solvents
MBG	Microbubble Generation Devices
PPGME	Polypropylene Glycol Methyl Ether
SBC	Sodium Bicarbonate Slurry
UNEP	United Nations Environment Programme
USD	United States Dollar

USD/MT	United States Dollar Per Metric Ton
w-%	Weight percent
vol-%	Volume Percent
WTE	Waste to Energy

Symbols

a	interfacial area	[m]
c_i^*	the solute concentration at the gas-liquid interface	[mol]
C_A^*	Concentration of dissolved gas at the interface, in equilibrium with the gas at the interface	[mol/mL ³]
C_B^0	concentration of reactant in the bulk of the solution	[mol/L]
c_{iL}	solute concentration in liquid bulk	[mol/L]
D_A	Diffusivity of the dissolved gas	[cm ² /s]
D_i	Diffusivity of component i	[cm ² /s]
E	Enhancement factor	[-]
F_B	Buoyancy force	[N]
g	gravity	[m/s ²]
$H_{CO_2}^{app}$	Apparent Henry's law constant	[kPa m ³ /mol]
H	Henry's law constant	[Pa]
Ha	Hatta number	[-]
J_i	Molar Flux	[mol/s]
K_2	equilibrium values	[mol/s]
K_G	Gas phase mass transfer coefficient	[cm/s]
k_{OH^-}	concentration based second order kinetic constant	[m ³ /kmols]
$K_{ov,G}$	gas phase overall mass transfer coefficient	[cm/s]
k_L	liquid side mass transfer coefficient	[cm/s]
$k_L a$	Volumetric Mass Transfer Coefficient	[1/s]
N	molar flux	[mol/s]
N_{CO_2}	moles of CO ₂	[mol/s]
P_i	Pressure of Component i	[kPa]
p	partial pressure of the solute in the gas phase	[Pa]

Q_L	Liquid flowrate	[L/min]
Q_g	Gas flowrate	[L/min]
r	rate of absorption	[mol/s]
Re_L	Reynolds number	[-]
r_b	bubble radius	[μm]
S	Solubility of CO_2 in water	[mol/L]
Sc	Schmidt number	[-]
Sh	Sherwood number	[-]
T	Temperature	[K]
X	Sodium/Potassium	[-]
x	mole fraction of the solute in the liquid phase	[-]
y	volumetric concentration	[vol-%]
\dot{v}	Volumetric flow rate	[m^3/s]
v_{sg}	Superficial gas velocity	[m/s]
ε_g	gas holdup	[-]
γ	activity of the component	[-]
ρ_G	gas density	[kg/m^3]
ρ_L	liquid density	[kg/m^3]
$\Delta p_{\text{CO}_2,LM}$	Logarithmic driving force	[kPa]
ΔC	change in CO_2 concentration at the gas- liquid interface and the bulk liquid	[mol/L]

Indices

<i>in</i>	inlet
<i>out</i>	outlet

1 INTRODUCTION

The alarming emission rates of the escalating greenhouse gases which is a crucial factor for the climate change needs a severe turn down. Power and heat producing industries and the energy use in transportation sector plays a high role in emitting these harmful gases. The interest with CO₂ has grown contemporarily from a mere waste to utilization and recently it turned out to be a solution from a problem in a sustainable and profitable way (Agency, 2019). More stringent and stronger calibre should be developed to curb or neutralize the dreadful consequences of climate change and if failed it will boost the momentum of global warming as the demand for energy rapidly increases. The idea of carbon neutral has the seed from circular carbon economy, by which CO₂ is transmuted into functional chemicals (Tracker, 2019).

In the UNEP report (2019), the change emission was 55.3 GtCO₂ (in 2018) of the global greenhouse gas emission rate with land-use. Accounting the Paris agreement, around 2.8 °C rise is estimated to reach around 2050 with global warming. IPCC in a special report (2018) the estimated carbon budget was 420 GtCO₂ by 2018 for a probability of 66% to circumvent the 1.5 ° Celsius rise in temperature of the globe. It is crystal clear by comparison that by any means of having a control on the global warming is very minimal (UNEP, 2019).

One of the prominent solutions to decrease the emissions is to capture and store CO₂, but the storage seems to be a bit difficult process since it involves heavy compression and excessive costs involved in capturing it. In base case CCS design which involves venting the by-product of CO₂ to atmosphere, combined with gasification-based configuration is the lowest cost of CCS although through gasification configurations more CO₂ is captured (Hannula and Melin, 2021). In Norway the Sleipner project which separates CO₂ offshore while extracting natural gas, sets as an example of geological storage of CO₂ in the underground cavities, which conceptualizes improving the gas and oil recovery potential by flooding it with CO₂. The *in situ* mineral carbonation seems an interesting alternate, injecting CO₂ in the underground reservoirs which reacts to form carbonates with alkaline minerals. Though geological storage and mineral carbonation is interesting the projects seem very minor scale when comparing the huge number of GtCO₂ produced and the latter technology has a very slow reaction which takes hundred thousand years to accomplish (Sipila.J, 2007). Although cost effective and more emission free energy spring from other alternates like solar and wind, a sudden wipe to the foundation of emission free or clean alternatives is challenging for the energy- intensive industries and global energy system. World- scale policy making and the stride of green

electrification infrastructure is deficient for the system to change rapidly into emission free and being inclusive in circular carbon economy (Nevander, 2021). Since the motif of renewable energy is inclining in contemporary times, the market value for adding carbon capture and storage (CCS) in bio-refinery flue gas streams would be in the range of 26 – 66 \$/tonne of CO₂. As a competitor to CCS, carbon capture and utilization (CCU) could be a promising move, since CCU enhances the output of the product but it is baffled by the variety of products which it can support (Hannula and Melin, 2021). CCU can be beneficial since the quantity of Carbon that is recycled today will be left underground for future generations which will not reach the atmosphere immediately and 10% of the total global emissions by 2030 could be reduced by with the help of CCU (Roberts, 2019)

1.1 Carbon capture, storage and its subsequent impact

Capturing CO₂ by any means is going to benefit the atmosphere and the direct solution to mitigate climate change, provided the production for CO₂ capture does not cause more GHG emissions than what are being captured. This carbon capture is not a new technology and geologic storage has happened much before in several industries across the especially earlier in western USA, Norway, Algeria, Canada (Barbara.P, 2009). Carbon capture and storage when coupled with biomass gives emission free and crucial in limiting the temperature rise to 1.5 °Celsius (Vinca, et al., 2018).

Carbon capture technologies has been mainly classified into three parts as post combustion, pre combustion and oxyfuel combustion technologies, by method of capture it can be classified into absorption, adsorption, membranes. Flue gas from power plants which almost contain 80% of nitrogen and 15% CO₂ has been let out as emissions. In post combustion, CO₂ is captured from flue gases produced by combustion. It is applied to major coal fired power plants and a favourable retrofit technology. Dilute in CO₂ concentrations, low CO₂ partial pressures are the most limiting factors for this technology.

In pre-combustion process, CO₂ is recovered from process streams before combustion or utilization. As the concentration and the pressure of the CO₂ containing stream can be increased to some extent in this process then the size and cost of the capture could be reduced. The potential to reduce the compression costs and more other options of technologies are available, seems as a plus for this technology. But in implementation extensive support systems and cost of the equipment seems to be a barrier of this technology.

To get higher concentrations of CO₂ in flue gas, oxygen is mixed with recycled flue gas and combusted which is popularly known as oxyfuel combustion. The recycled flue gas work as a heat carrier and thus reducing the flame temperature. The repowering technology option and large cryogenic O₂ production equipment seems to be the advantages and limitations respectively in large scale manufacture (Figuerola, et al., 2008).

CO₂ capture by post combustion process which is the most supported technique since it is a backfitted model to the existing units of power plants. Typically, the power plant flue gases has a concentration of 4 to 14% of CO₂ and released in the atmospheric pressure which as a result has low thermodynamic driving force for CO₂ capture and large volume of gas has to be captured. In a post combustion capture of CO₂, aqueous sodium hydroxide solution was used in a series of continuous reactor system containing a bubble and packed bed column, the following observations were made. The idea is to produce sodium bicarbonate by capturing CO₂ from powerplant flue gases using sodium hydroxide. Optimal design parameters of the columns were determined which could be used in scale up of this process and an absorption rate of 95% was achieved. However, the most influencing operating parameters is the concentration of the liquid absorbents, continuous supply of fresh hydroxide to react with the injected CO₂ is the prime parameter which makes sure that there is sufficient absorption (Shim, et al., 2016).

1.2 E-Fuel Production

Since the global market is highly dependent on conventional fuels especially fossil hydrocarbons which should be avoided in near future at the same usage intensity if the climate targets have to be reached. CCU and CCS are the powerful technologies in reaching these targets. As a substitute for fossil fuels, regenerative fuels especially the e-fuels derived from hydrogen and CO₂ could replace at least half of the fossil fuels before facing the shortages. The time for transformation to other alternatives which are feasible has already arrived and e-fuels will only become competitive only if the conventional fuel established structures break down and all policyholders move towards a sustainable approach (Schneider, 2019).

The advantage of e-fuel originates from easy storage and high energy density when compared to conventional fuels. Electricity from renewable energy sources, water and CO₂ from industrial exhaust gases or from air is used in the production of e-fuels. Through electrolysis, hydrogen is produced and combined with CO₂ produced from air or from industrial exhaust

sources with the help of Fischer-Tropsch synthesis, involving high pressure and usage of catalyst, resulting in a liquid energy carrier, extensively this procedure is known as power to liquid process.

The main challenge that e-fuel production tackles is that the storage of excess energy which is produced from renewable power production and its proportion to be used for e-fuels manufacturing (Ausfelder and Wagemann, 2020).

1.3 BECCU

BECCU (Bioenergy with Carbon Capture and Utilization) uses CO₂ as a feedstock and converts it into value-added products such as synthetic fuels, chemicals or food and beverages or building materials. Through BECCU the captured carbon from a biomass energy conversion can be recycled via chemical or biological processes to form biochar, synthetic fuels and construction materials through mineralization. Primary difference between BECCS (Bioenergy with Carbon Capture and Storage) and BECCU is that BECCU enables the economic use of CO₂ through temporary storage with possible re emissions of CO₂ at the end. In Finland the project BECCU is to accomplish a framework with proof of integrated production of bio-based chemicals and fuels, heat and power which is financed by Business Finland (Nevander, 2021). The E-Fuel's project in Finland was launched by February 2021, which aims in boosting the synthesis concept of e-fuels and the commercial readiness for high temperature electrolyzers closer to low temperature level technologies (VTT, 2021).

2 OBJECTIVE

The objective in this thesis was determine the local mass transfer rates, needed residence time in CO₂ – sodium carbonate system to reach desired CO₂ capture efficiency. Also, to determine the overall mass transfer rate of CO₂ dissolution in enhanced soda scrubbing process using microbubble generator as a function of liquid and gas flow thereby obtaining the optimal process conditions as trade-off between pumping energy input and mass transfer efficiency.

Also to create a calculation model which is used to estimate the performance of the process as function of residence time and flowrate of liquid, gas.

LITERATURE REVIEW

3 REVIEW ON CO₂ CAPTURE PROCESSES BASED ON CARBONATES

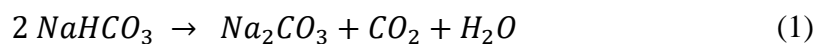
The most commercially evolved liquid absorbents to capture CO₂ are amines which are derivatives of ammonia containing nitrogen-organic compounds. Amines have excellent chemical properties namely good reversibility, higher reaction kinetics. Usually the mono ethanol amine (MEA) and diethanol amine (DEA) were used to capture CO₂ from the flue gas, since the amine solutions are corrosive to the equipment and needs high energy cost for regeneration of steam. Supported amine absorbents are a way to reduce corrosivity and regeneration energy, but the raw materials seem very much expensive to be used in a large-scale application (Cai, et al., 2018).

Aqueous sodium carbonate solutions has a potential to be both cost effective and energy efficient in CO₂ capture. The main barricade in using carbonate solutions is their slow reaction kinetics.

To address this problem, Na₂CO₃ powders were dispersed on solid supports which resulted in vain by reducing the sorption capacity of CO₂, which in turn decreases the amount of active components per unit mass due to the inclusion of supports. To overcome this in an experiment support free hydrated sodium carbonate powders (HSCPs) were prepared by mixing water and sodium carbonate powders. The mixture solution as a result of dissolution of partial Na₂CO₃ is freely attached into the hydrated Na₂CO₃ particles, thereby giving high gas-liquid interface for CO₂ capture which in turn reduces the overall cost of raw materials and also increases the sorption capacity. The inference from the results of the experiments was influenced by the form and structure (morphology) of the HSCPs. When the concentration of the Na₂CO₃ is low, the appearance of the HSCP is aqueous or slurry which is not perfect for CO₂ capture due to low gas-liquid contact surface area (Cai, et al., 2018).

3.1 Waste Incinerator- CO₂ Capture and re-use

In a newly developed process in eastern part of Netherlands, they used pure CO₂ stream to produce sodium bicarbonate (SBC) slurry instead of the prevailing techniques like using SBC particles (Cai, et al., 2018). This is the only process which has the idea of closed CO₂ cycle with respect to flue gas cleaning. In flue gas the acidic impurities are removed by introducing buffered SBC via injection nozzles together with steam. When the hot flue gases are in contact with sodium bicarbonate by the following reaction sodium bicarbonate breaks down to SBC (Na₂CO₃) which is an endothermic reaction.



The SBC slurry is produced from the NaCO_3 solution formed by dissolving solid soda in water with a separate soda dissolve unit and an innovative reactor configuration is used to convert sodium carbonate (30 w-% solution) to SBC (40 w-% slurry= \pm 35 w-% solids) with CO_2 (pure gas) produced by burning fossil fuels and some excess amount of CO_2 is also required for sodium bicarbonate production.

The 40 w-% SBC is produced in order to minimize the temperature drop of the flue gas. The sodium carbonate is produced from the green CO_2 which is produced at the waste incinerator thus a closed CO_2 cycle is obtained, another big advantage of this process is its negative carbon footprint.

Also sodium bicarbonate being an expensive product (297.77 USD/MT) (Qingdao Echemi Technology Co., 2018) it is produced beneficially because 1 ton of carbonate can produce 1.6 ton of bicarbonate which is more valuable than carbonate of same quantity. The flue gas after introducing to SBC slurry, CO_2 and a Na_2CO_3 particle with large specific area is formed is released in the flue gas channel in which Na_2CO_3 reacts with the acidic impurities present in the flue gas.

The flue gas is routed to quench where it is cooled and the pH of the quench liquid is maintained by adding a pinch of concentrated sodium carbonate from the soda production unit and acidic impurities present in the flue gas of lower concentrations are removed.

The impurities removed and cooled flue gas is directed to CO_2 capture installation where pure CO_2 is produced by using a biodegradable solvent Bilisol which is low in degradation rate and very low in volatility. The pure CO_2 stream is directed to 2 stirred tanks, reactors connected in series (chosen to connect in series because of high mass transfer rates) where SBC slurry is produced using sodium carbonate solution from soda dissolve unit.

As such for amines, CO_2 reacts with Bilisol solvent in a similar way of regenerative acid-base reactions in the liquid phase and the regeneration of the solvent is very efficient due to the usage of low grade heat used from waste to energy (WTE) plant.

In overall, to estimate the reaction regime Hatta number was calculated where the rate of the reaction in the liquid film is compared to the diffusion rate through the film, which was below 1 and the inference is reaction rate is slow compared to mass transfer. Up to 2000 ton per year

of CO₂ from flue gas is captured from SBC which is 8000 tons of sodium bicarbonate produced annually (Huttenhuis, et al., 2016).

3.2 Vartan Bioenergy Plant- Idea

In another case, Stockholm Exergi AB has inspired from BECCS concept where the idea is to compress CO₂ into liquid state and reposit in underground rock formations when reaching full scale operation. And plans to install full scale capture system into the existing biomass-combined heat and power plant which is a path towards creating carbon sink in Stockholm. A roof top rig is planned in the Vartan complex to extract flue gases and Stockholm Exergi preferred to go with Hot potassium carbonate process. The technology used here is based on Sargas Process, a simple form of Benfield process which is developed to remove compounds like CO₂ and H₂S. It is configured by hot potassium carbonate process, where CO₂ and H₂O react with hot potassium carbonate (HPC) under pressurized conditions thereby forming bicarbonate which is then led to a desorber column where carbonate is regenerated by reducing pressure (Levihn, et al., 2019). The idea from a BECCS plant would be a great advantage here because of the reuse of excess heat within one CHP. 800000 tonnes per annum of CO₂ will be the potential estimated capture in Vartan and 2 million tonnes annually from whole of Stockholm (International, 2019).

3.3 Microencapsulated liquid sorbents for CO₂ capture

Highly permeable, microencapsulated carbon sorbents (MECS) is used to capture carbon which has a combined advantage of liquid solvents (i.e., high capacity, selectivity, water tolerance) and solid sorbents (high surface area, low volatility). The desired product is achieved when the CO₂ from flue gas diffuses through the thin capsule shells, then dissolves and reacts in the liquid sorbent. The regeneration is achieved by heating where high purity CO₂ is yielded back, which can be later compressed and stored for utilization. Silicone shell is chosen an encapsulating material after broad examination in terms of photo curable and chemically compatibility with the sorbent. The idea of encapsulating the carbonate sorbents (either potassium or sodium carbonate solution) overcome their own main drawbacks of slow CO₂ absorption kinetics and difficulty in handling precipitated solids.

The MECS are produced using a double capillary device. The capsule consists 2 layers or shells, the core contains the aqueous carbonate solutions with or without a pH indicator dye and catalyst for enhanced CO₂ sorption. The core capsule shell is a photopolymerizable silicone and the outer layer consists of an aqueous solution with surfactant and stabilizer. But when

capsules are packed randomly it creates high pressure drop for gas flow, supported packing which creates channels for flow or a fluidized bed is recommended.

When the MECS with liquid sorbent turns yellow when the maximum carbon uptake is achieved which serves as an indicator of CO₂ saturation of the liquid carbonate sorbent also as an monitor for capsules loading and unloading. Experiments were performed to test the cycling and mechanical integrity and the results indicate that the shell material retains its permeability. Osmotic swelling in water was tested to have an idea about mechanical stability and crystallization, up to fourfold increase in diameter was withstood by non-ruptured MECS. The correlation between the predicted and measured mass transfer rate was inline. Also altering the geometry of the capsules can increase two times the surface area (Vericella, et al., 2015).

3.4 Promoted CO₂ capture using Bio catalyst

Integrated Vacuum Carbonate Absorption Process (IVCAP) which involves aqueous potassium carbonate solutions for CO₂ absorption. IVACP uses the waste or low-quality steam from the power plant's low-pressure turbine to give the stripping heat since the heat of absorption of CO₂- potassium carbonate system is much less when compared to other absorbent systems, weak affinity between CO₂ and potassium carbonate makes CO₂ to be desorbed from CO₂ rich solution at lower temperatures and pressures. The temperature and the pressure at the stripper are 50-70°C and 0.13-0.55 bar. The vacuum is obtained by condensation of water vapour from CO₂ and partially by vacuum pump. Technically additional energy is required for vacuum pump but the usage of low quality steam from powerplant in combination with low heat of absorption between CO₂ and potassium carbonate solution might result in 20-35% lower overall energy consumption when compared to MEA based processes. The barricading factor is the absorption kinetics and to improve many solvents were mixed with stronger affinity with CO₂ which ultimately increases the overall energy consumption of the process. And using catalyst to promote the absorption rates does not work with improving the heat of absorption. Catalysts such as arsenite, sulphide, hypochlorite formaldehyde was studied for catalysing but resulted in release of toxins and high corrosivity. A CO₂ hydration catalyst carbonic anhydrase enzyme has been used as a catalyst and the activity was tested by parametric tests.

The measurements were performed in batch mode in a continuous stirred tank reactor and the change in composition of liquid phase is negligible during absorption since large volume is taken into account, the system was vacuumed to strip off moisture and other gas contents and then the system was allowed to stabilize. The experiments were performed and from the results

it can be inferred that the absorption rates were higher when compared to CO₂-MEA system with potassium carbonate – carbonic anhydrase enzyme system (Lu, et al., 2011).

4 PHENOMENA IN SODA BASED CO₂ CAPTURE

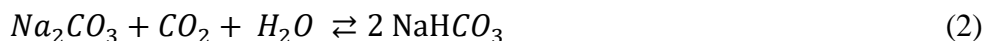
4.1 Chemistry in soda-based CO₂ capture

The basic chemistry involved in CO₂ capture via carbonate solvents is by chemical absorption. Chemical absorption which means the chemical reaction between substance to be absorbed and the absorbing medium. In this case the substance absorbed is CO₂ and absorbing medium is carbonate solution. The basic idea of capturing CO₂ by carbonate solutions is that it forms a weakly bonded intermediate compound which can be regenerated with the application of heat and producing back the original solvent (Wanga, et al., 2011).

4.2 Chemical Reactions

4.2.1 Overall reaction

The overall reaction can be represented by (2)



The chemical absorption of CO₂ in carbonate solutions can be represented by two major reaction steps (3) and (4) (Green, et al., 2004) (Knuutila, et al., 2010)

Step 1:



Step 2:



In step 1 the CO₂ is reacting with hydroxide ions to form bicarbonate ions with weaker bonding so that in the next step the bicarbonate ions again reacting instantaneously gets back to release carbonate ion and water. (Hikita, et al., 1976)

4.3 Gas solubilities by Henry's law

The rate of the gas which is being dissolved in the absorbent liquid is influenced when there is a variation in the equilibrium of the system, which presses to consider the equilibrium characteristics of gas-liquid systems. In this case it is two-component system in which the resultant concentration of the dissolved gas (absorbent- CO₂) in the liquid (absorbate- Na₂CO₃)

is known as the gas solubility at the corresponding temperature and pressure is available. In general, the solubility of the gases are influenced by temperature to some extent (Treybal, 1981). The Henry's law states that

$$p = Hx \quad (5)$$

where p - partial pressure of the solute in the gas phase (Pa), x -mole fraction of the solute in the liquid phase, H -Henry's law constant (Pa) (Branan, 1999).

It is much essential to know the solubilities of gases to estimate the gas-liquid mass transfer rate which is possible only by knowing the volumetric mass transfer coefficient and also the equilibrium liquid-phase concentration. In an attempt to measure the solubilities of CO₂ in potassium carbonate solutions N₂O was used instead of CO₂ to avoid chemical reactions (Knuutila, et al., 2009) and also the physical solubility is established based on the solubility of CO₂ and N₂O in water (Weisenberger and Schumpe, 1996) (Hermann, et al., 1995).

To estimate the solubility, accurate density measurements are necessary which was measured by 25 ml calibrated pycnometers from 298 K to 353 K (Knuutila, et al., 2010).

The solubility of N₂O was established experimentally by using a stirred jacketed glass reactor and a stainless steel gas holding vessel setup. The obtained solubility was well in line with the models of Weisenberger and Schumpe. The Henry's law constant was established and Figures 1 and 2 represents the Henry's law constant.

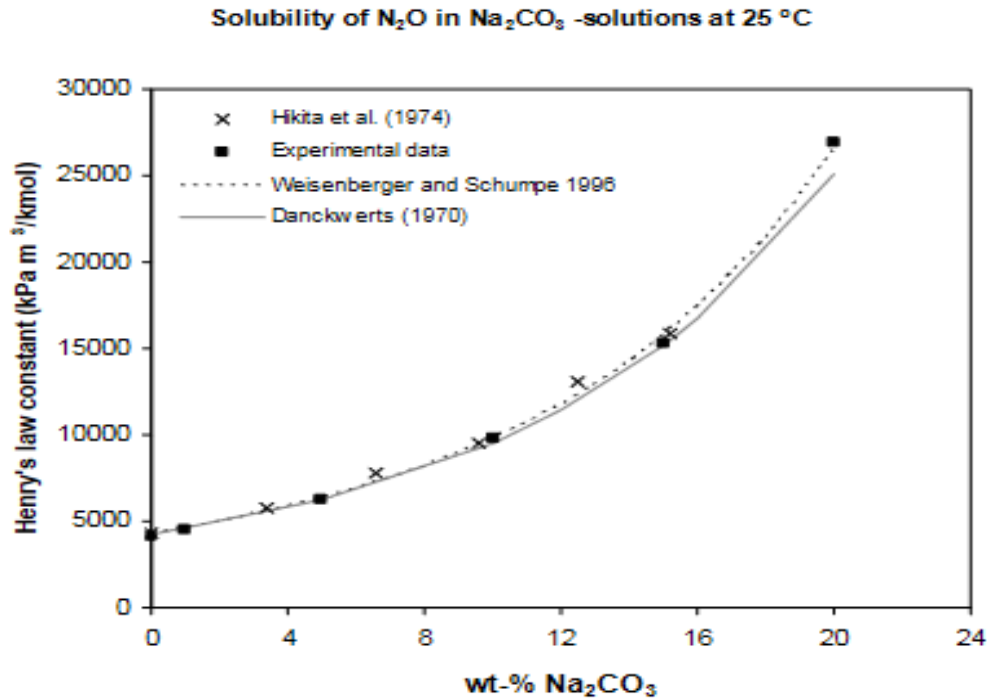


Figure 1 Henry's law constant for N_2O in sodium carbonate solution at temperature of 25 °C (Knuutila, et al., 2010)

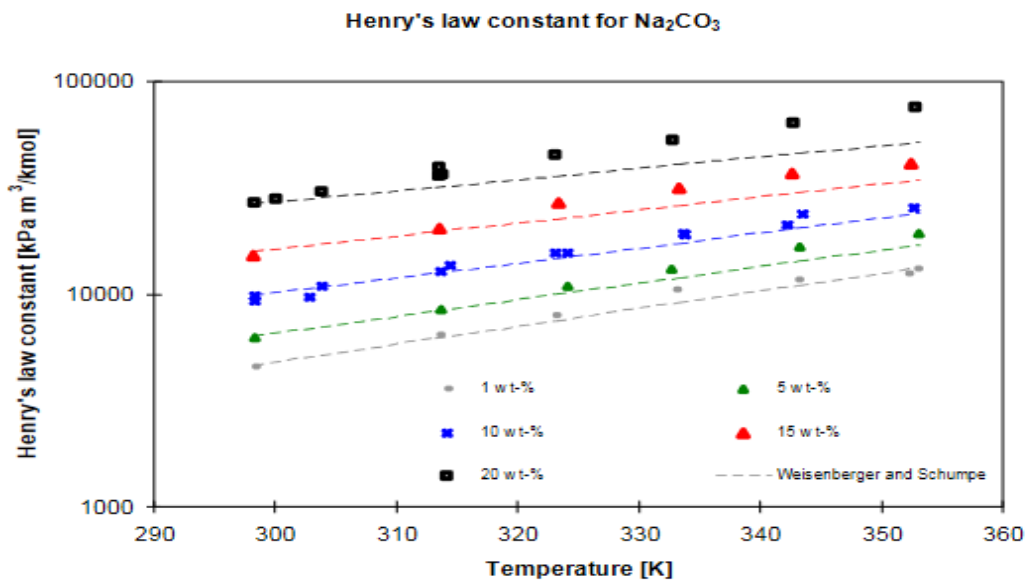


Figure 2 Henry's law constant for N_2O into sodium Carbonate solutions (Knuutila, et al., 2010)

The apparent Henry's law constant can be used to calculate the liquid phase concentration of CO_2 by Equation (6) (Knuutila, et al., 2010)

$$H_{CO_2}^{app} = \frac{P_{CO_2,i}}{[CO_2]_i} \quad (6)$$

4.4 Kinetics of CO₂ absorption in soda-based solutions

The Equation (3) in the whole process is the rate determining step because Equation (4) is just a proton transfer reaction and the rate equations are based on OH^- due to the lower concentrations of CO_3^{2-} in the solution. It should also be noted that the concentration of OH^- ions are determined by the base constant. The rate equations are as follows and the methods, apparatus used to measure the kinetics is described in section 6.

$$r = k_{OH^-} [OH^-] [CO_2] \quad (7)$$

Rate equation based on activity

$$r = k_{OH^-}^Y [OH^-]_Y [CO_2]_Y \gamma_{CO_2} \gamma_{OH^-} \quad (8)$$

Where k_{OH^-} is the concentration based on second order kinetic constant (Knuutila, et al., 2010).

In another case where the rate equation was obtained for CO₂ reacting with sea water and the equation is as follows,

$$\begin{aligned} \frac{d[CO_2]}{dt} = & (k_{CO_2} + k_{OH^-} [OH^-]) \cdot [CO_2] \\ & + (k_{CO_2, r[X^+]} + k_{HCO_3^-}) \cdot [HCO_3^-] \end{aligned} \quad (9)$$

in any case the correlation between the sea water and soda solutions would be just the change of cations, so in the place of X we can replace by sodium or potassium (Emerson and Hedges, 2008).

5 MASS TRANSFER

In general terms mass transfer describes the transfer or movement of mass or matter from one stream to another. This mass transfer might involve in a single phase or over phase boundaries in multiphase systems. Absorption is a branch of mass transfer in which absorbate is being absorbed by a liquid absorbent (cyclopedia, 2015) (Perry and Green, 1997).

5.1 Theory of mass transfer

There are 3 different theories which deals with mass transfer among phases viz. two-film theory, penetration theory and surface renewal theory. The oldest and a well-developed theory by Lewis Whitman would be two-film theory (Morsi and Basha, 2015). The theories are all

based on how the diffusivity occurs in different phases. In case of gas absorption, solute diffuses through the gas phase reaching the interphase between the phases and then to the liquid phase from the interphase. This diffusion is caused mainly by the difference in the concentration gradient which makes the component to move in such a direction so that it equalizes concentration by destroying the gradient (McCabe, et al., 1993)

5.2 Mass Transfer rate

In steady-state mass transfer, flux through the liquid film is described by equation (10)

$$J_i = k_L a(c_i^* - c_{iL}) \quad (10)$$

where c_i^* represents the solute concentration at the gas-liquid interface, c_{iL} is the solute concentration in liquid bulk, k_L is the liquid side mass transfer coefficient and a represents the gas-liquid interfacial area (Morsi and Basha, 2015). This mass transfer rate in turbulent flow does not prevail as same because there is an increase in rate of transfer per unit area by creating more interfacial area (McCabe, et al., 1993).

In an attempt to measure the CO₂ absorption rate using DOWFROTH 200 (explained in section 7.1), the equation (11) was utilized which relates the gas-liquid interfacial area, concentration gradient, liquid side mass transfer coefficient to the rate of CO₂ absorption into the carbonate solution

$$r = k_L a \Delta C \quad (11)$$

Where, r – rate of absorption, k_L – liquid side mass transfer coefficient, a - gas- liquid interfacial area, ΔC - change in CO₂ concentration at the gas- liquid interface and the bulk liquid (Spigarelli, 2013).

5.3 Film Theory

The transport of mass within a single phase depends directly on the concentration gradient of the transporting species, when mass transfer happens between one phase to another phase, called as interphase mass transfer. Film theory is a simplification of real phenomena which enables us to estimate mass transfer rates between different phases

The concept of film theory was borrowed from the convective heat transfer idea. When a fluid flows turbulently past a solid surface, with mass transfer occurring from the surface to the fluid, the concentration-distance relation is gradual which is represented by the Figure 3. The shape

of the curve is controlled by varying the ratio of Eddy mass transfer diffusivity E_D and diffusivity D . C_{A1} and C_{A2} are the initial and final concentrations, Z_F - film thickness.

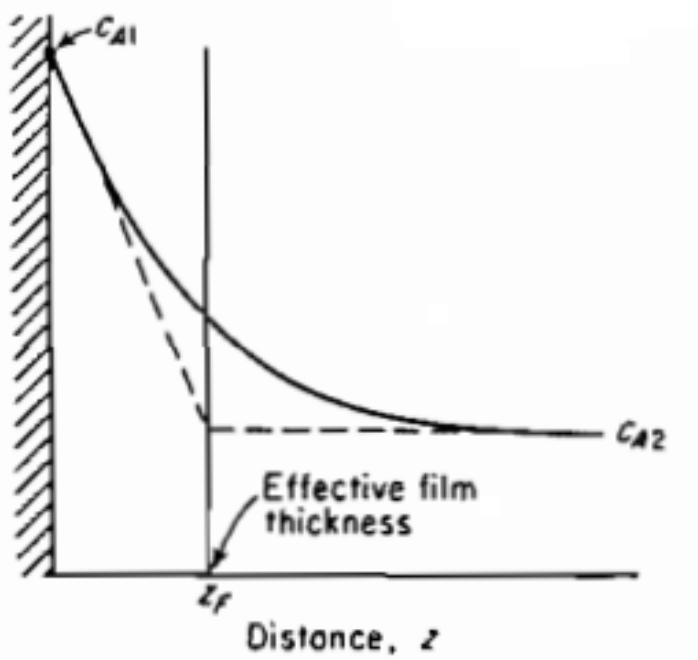


Figure 3 Concentration Distance Relation, Film Theory (Treybal, 1981)

But this film theory is in conflict for the turbulent flow processes due to the much smaller dependency in diffusivity and also poor in handling the effect of high mass transfer-flux and in predicting the effect of chemical reaction rate on mass transfer (Treybal, 1981).

5.4 Two-Film Theory

Transport between two phases requires a departure from equilibrium and the equilibrium of transporting species is of primary concern. The general theory has two principal assumptions:

1. The rate of solute from gas phase transfer between the phases is controlled by the rates of diffusion through the phases on each side of the interface.
2. The rate of diffusion of solute across the interface is instantaneous and therefore equilibrium at the interface is maintained all times

In simpler terms only diffusional resistances are those residing in the fluids themselves. In general, the solute diffusing from the gas phase to the liquid possess a concentration gradient in the route of mass transfer within each phase (Treybal, 1981). The break at the interface makes mass transfer between two phases more complex. This is caused due to the in equal

mole fraction or concentration present on both the sides of the interface. In case is the absorbing gas is very soluble the mole fraction of the liquid at the interface will be greater than that in the gas which is represented by Figure 4.

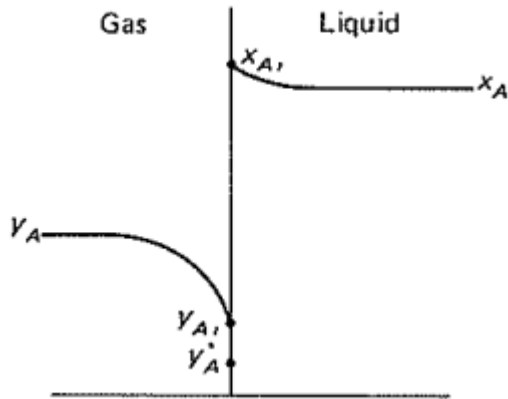


Figure 4 Absorption of a very soluble gas (McCabe, et al., 1993)

Where x_A and $x_{A,i}$ are liquid side mole fractions and y_A , $y_{A,i}$, and y_A^* are gas side mole fractions (McCabe, et al., 1993). In this theory the mass transfer is treated as a steady state process and so the theory is applicable only if the required time for the concentration gradients to become established is small comparing to the time of transfer (Coulson, et al., 1999). The steady state absorption of CO_2 by two film theory can be stated by Equation (12)

$$N_{\text{CO}_2} = K_G(P_{\text{CO}_2,b} - P_{\text{CO}_2,i}) = Ek_L^0(C_{\text{CO}_2,i} - C_{\text{CO}_2,b}) \quad (12)$$

When the reaction happens in the film mass transfer is enhanced and so we used enhancement factors in the calculations.

5.5 Mass transfer coefficients of gases and liquids

The mass transfer coefficients are defined as the rate of mass transfer per unit area per unit concentration difference, usually represented by k (McCabe, et al., 1993).

In an experiment performed by Hanna Knuutila to measure the kinetics of CO_2 in aqueous sodium carbonate solution a string disc apparatus was used. Using the known dimensions of the rotating disc and active mass transfer area the flux was calculated from which the kinetic parameters are estimated (Knuutila, et al., 2010) (Ma'mun, et al., 2007).

In general the molar flux is proportional to the concentration difference, if individual (one dimensional) flux are considered then mass transfer coefficient is represented separately for

gas and liquid phases. Table 1 which represents the mass transfer coefficient for different superficial gas velocities for CO₂ and aqueous sodium carbonate solution.

Table 1 Represents the experimental results of gas superficial velocities and $k_L a$ for reaction with Na₂CO₃ and CO₂ (Ajay Mandal, 2003)

v_{sg} (m/s)	D_N (m)	$\alpha_1 k_2 C_B^0$	$\frac{D_A k_2 C_B^0}{k_L^2}$	$K_1 a$ (s ⁻¹)
0.042	0.004	2.72	0.0293	0.096
0.044	0.004	2.82	0.0294	0.105
0.0501	0.005	2.56	0.0214	0.123
0.053	0.005	2.72	0.016	0.146
0.028	0.006	1.70	0.017	0.066
0.032	0.006	1.67	0.020	0.079
0.015	0.007	1.94	0.175	0.044
0.0202	0.007	2.08	0.009	0.067

5.6 Enhancement Factor

The enhancement factor which is defined as the ratio of the flux of absorption in the presence of pure chemical reaction to the flux of pure physical absorption. Also, the number of times the physical absorption flux is enhanced by chemical reaction is the enhancement factor. The enhancement factor for an instantaneous reaction is independent of the mass transfer coefficient k_L or the hydrodynamic conditions (film thickness) which can be verified experimentally (Hosten, 1984). The equation used to calculate the enhancement factor from two-film theory is stated below (Knuutila, et al., 2009)

$$E = \frac{Ha}{\tanh(Ha)} \quad (13)$$

And the definition of Hatta number is given by the following equation

$$Ha = \frac{\sqrt{k_1 D_{CO_2}}}{k_L^0} \quad (14)$$

6 MEASUREMENT OF MASS TRANSFER IN CO₂-CARBONATE SYSTEM

6.1 Attempt to measure interfacial area

For gas–liquid processes that happens in the absorption regime with a slow reaction, the mass transfer properties can be clearly characterized by volumetric mass transfer coefficient and the knowledge about gas-liquid interfacial area, volumetric mass transfer coefficient will be of great use in designing and scaling up of a gas-liquid reactor. The flow conditions and other

parameters will also determine the needed size of the system and to achieve a range of performance.

In this experiment a concurrent down flow bubble column with microbubble generator type gas-liquid distributor is used to measure the interfacial area and volumetric mass transfer coefficient. A plunging jet type is used to produce high velocity liquid jet through the nozzle which touches the surface of the liquid and pierces into it. The gas is separated from the liquid at a separation chamber situated at the bottom. Pressure in the separator and liquid level is used as a caliber to adjust the size of the gas-liquid mixture in the contactor. An intense gas-liquid mixing zone and homogenous gas-liquid zone were observed in the contactor. In the first zone the liquid jet penetrates the liquid and releases its energy to disperse the gas, a minimum liquid flowrate is required to move the gas bubbles downwards or else it would circulate in the column due to their high buoyant force. A heterogeneous slug flow appears when the liquid flowrate is increased over a certain limit.

Sodium hydroxide solutions (primary fluid) of desired compositions was used to measure the interfacial area and sodium bi carbonate solution (secondary fluid) was used to measure liquid-side volumetric mass transfer coefficient. By pumping the primary fluid via nozzle and dispersing the secondary fluid by jet momentum a two-phase mixture is obtained and moved through the contactor by transferring of the solute gas into the liquid phase. After the system reached the steady state the parameter values were noted and the gas, liquid samples were collected at the sampling point for further analysis. The specific interfacial area was obtained by the knowledge of diffusivity of CO_2 in aqueous solutions, rate constant and Henry's law constant. Rate of mass transfer per unit volume and interfacial concentration of carbon dioxide is used in measuring the liquid-side mass transfer coefficients. As a result of increased turbulence there is an increase in volumetric mass transfer coefficient, with an increase in the liquid flowrate. As a conclusion, two correlations were developed as a function of superficial gas velocity with volumetric mass transfer coefficient and gas liquid interfacial area (Mandal, et al., 2003).

6.2 CO₂ absorption rates by wetted column and string of disc apparatus

6.2.1 Equilibrium Measurement

Aqueous sodium carbonate solutions were prepared using deionized water. The measurement of vapor-liquid equilibrium was tested in the VLE apparatus for atmospheric pressure. Equilibrium in the system was achieved when the gas analyzer showed same CO₂ values. Partial pressure of CO₂ in the system was calculated using the temperature, mole fractions. Ebulliometer was used to estimate the water vapor pressure over aqueous sodium carbonate solution. Modeling of vapor-liquid equilibrium was performed and the results show that it is impossible to reach zero conversion to bicarbonate using aqueous sodium carbonate solutions (Hessen.T, et al., 2010).

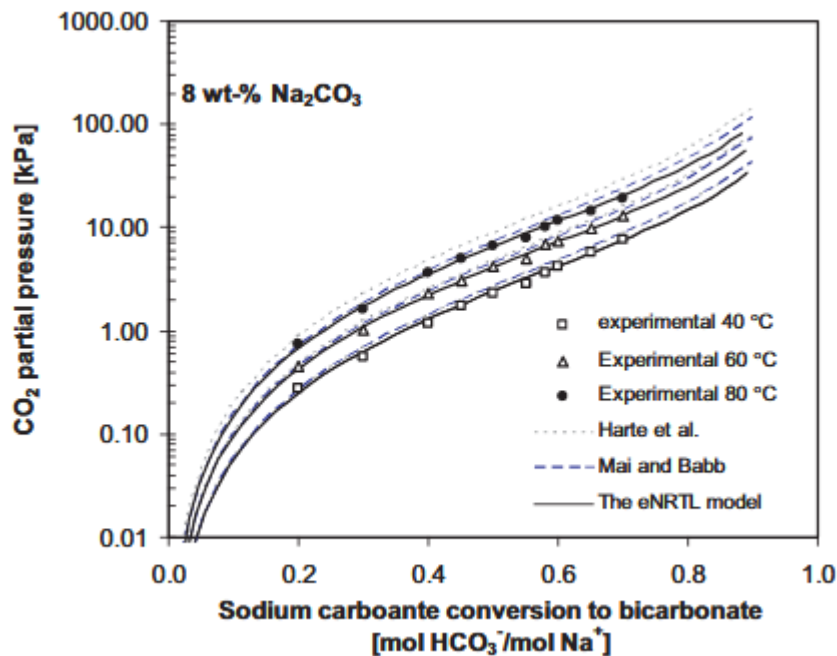


Figure 5 Partial pressure of CO₂ as a function of sodium carbonate conversion to bicarbonate using 8w-% sodium carbonate solution (Hessen.T, et al., 2010).

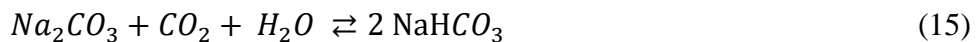
In another attempt which involves two stages, in stage one flue gas is exposed to an aqueous solution of Na₂CO₃ which favors formation of NaHCO₃, in which the CO₂ from the flue gas is kept in liquid as sodium bicarbonate and in the second stage the liquid is in contact with the flue gas which inclines to decomposition of NaHCO₃ to sodium carbonate, CO₂ and water as vapor.

An equation which depicts equilibrium relationship between the variables was developed by McCoy and Smith (McCoy and Smith, 1911) which was utilized to obtain the value of

numerical coefficient to get an equilibrium relationship between fraction of sodium in form of bicarbonate (X) and its partial pressure .

The determination of numerical coefficient helped in, 1) establishing equilibrium at different temperatures between a liquid phase having desired sodium normality and a gas phase having a known partial pressure of CO_2 , 2) analyzing the liquid phase, determine the equilibrium concentrations of Na_2CO_3 and $NaHCO_3$.

In the experimental part the air and CO_2 desired combination was fed using the help of capillary flowmeters to the mixing chamber. To ensure saturation of the air with water vapor and to maintain its temperature a humidifier and heater was used and tested using wet-bulb and dry-bulb thermometers. Wetted wall type tower was used to perform the experiment. Only the liquid stream in the experiment was circulated using a pump and the gas stream was let out after a single pass. The equilibrium was attempted as a continuous process and batch process for gas and liquid phases respectively. Different concentrations, temperature of the liquid and different gas compositions was tested at least for two runs. Equilibrium was approached for the Equation (15)



Samples was obtained every 30 minutes and the liquid samples were analyzed to determine the sodium concentration and fraction of sodium in the form of bicarbonate. The modified Winkler method was used to determine the carbonate and bicarbonate concentrations which involves utilizing standard barium hydroxide solution, precipitating the carbonate out and titrating it back by standard acid which gives the measure of bicarbonate concentration using phenolphthalein and methyl orange as an indicator.

$$M = 20 (185 - T) C^{-0.29} \quad (16)$$

Where, T – temperature in $^{\circ}C$.

Equation (16) is used to obtain the value of M which is described as numerical coefficient in establishing equilibrium relationships (C.R Harte, et al., 1933).

6.2.2 Mass transfer measurement

In attempt to measure the kinetics of sodium and potassium carbonate solution a sting of discs apparatus was used, represented in Figure 7

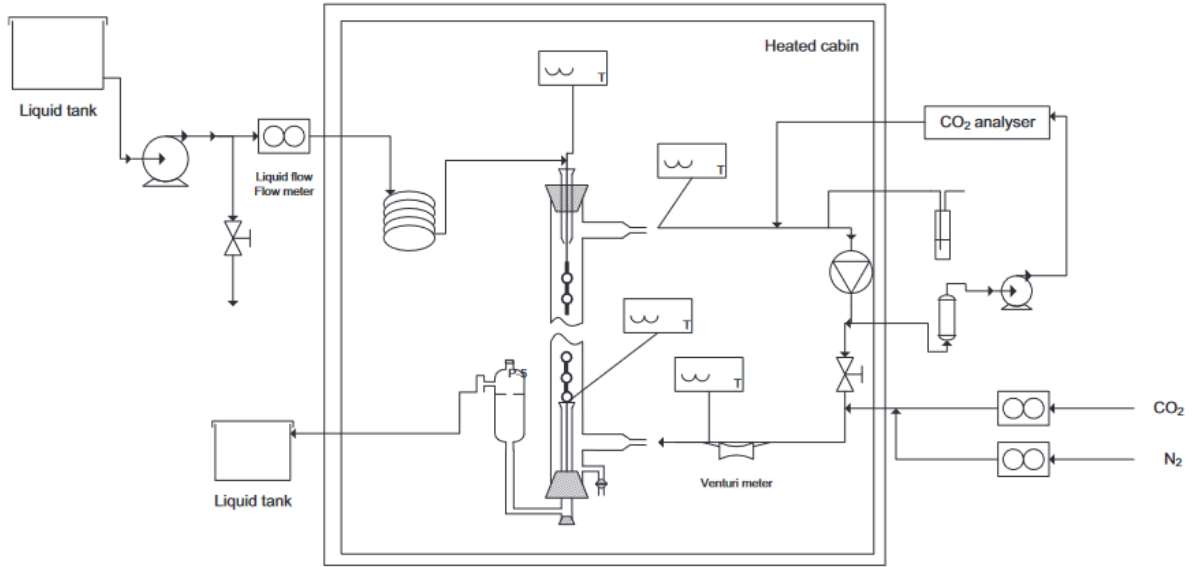


Figure 6 Experimental setup of spring disc apparatus (Knuutila, et al., 2010)

5 to 30 weight percent of sodium carbonate solutions were used at temperatures between 25 to 70 °C, the system was operated in counter current manner so the liquid was entering from the top and removed at the bottom through a small funnel while the gas entered from the bottom through a long disc (to establish a pattern) and exits from the top. Both the liquid and gas flowrates were adjusted separately. The concentration of the gas was also controlled by mass controllers and a constant pressure was maintained throughout. Both liquid and gases (CO₂ + N₂) were allowed to react until constant values were reached (deemed as steady state process). Data was acquired and average values were calculated. Overall mass transfer coefficient was obtained by Equation (17) In an experiment with string of discs apparatus the gas phase overall mass transfer coefficient was established using the following equations

$$K_{ov,G} = \frac{N_{CO_2}^{in} - N_{CO_2}^{out}}{\Delta p_{CO_2,LM}} \quad (17)$$

Where $K_{ov,G}$ - gas phase overall mass transfer coefficient, $N_{CO_2}^{in}, N_{CO_2}^{out}$ – moles of CO₂ fed and out of the system respectively, $\Delta p_{CO_2,LM}$ – logarithmic driving force over the string of discs. Logarithmic driving forces are determined by calculating logarithmic mean between inlet and outlet equilibrium pressures of CO₂ over the liquid at inlet and outlet. The overall mass transfer coefficients can be calculated (without modelling and based on absorbed CO₂) using the following equation (Knuutila, et al., 2010).

$$K_{ov,G} = \frac{1}{\frac{1}{k_G} + \frac{H^{app} CO_2}{Ek_L^0}} \quad (18)$$

Ajay Mandal et al experimented to determine the interfacial area and liquid side volumetric mass transfer coefficient (mass transfer by chemical reaction) in a downflow bubble column by absorbing CO₂ in sodium hydroxide and sodium carbonate/bicarbonate solution was tested with an microbubble generator which serves both as a sparger and plunging jet. The conditions for equation (3) and (4) was tested based on OH⁻ concentration which needs to be constant in the bulk of the solution so that equation (3) turns to be pseudo first order and the condition is as follows

$$\left[\frac{D_A K_2 C_B^0}{k_L^2} \right]^{\frac{1}{2}} \ll 1 + \frac{C_B^0}{2C_A^*} \quad (19)$$

The specific rate of absorption per unit area for a second order reaction which satisfies the above-mentioned condition is given in the below equation

$$R = C_A^* \sqrt{D_A k_2 C_B^0 + k_L^2} \quad (20)$$

and if

$$\left[\frac{D_A K_2 C_B^0}{k_L^2} \right]^{\frac{1}{2}} > 3 \quad (21)$$

the equilibrium value (k_2) becomes small compared to the diffusivity of CO₂ in equation (20). And also when the conditions (19) and (21) are satisfied the absorption rate will be a function of physiochemical factors and will be independent of the hydrodynamic conditions. However, the system was tested only for sodium hydroxide solutions, only the cations will be different in the sodium carbonate/ bicarbonate solutions which is of close resemblance with this tested system. The conditions would be applicable to our experiments also and it is possible to find out using the criteria under which the hydrodynamic behaviour of the system does not affect gas dissolution speed.

The correlation for the interfacial area with the superficial gas velocity is given by equation (22)

$$a = 0.38 \times 10^4 v_{sg} \quad (22)$$

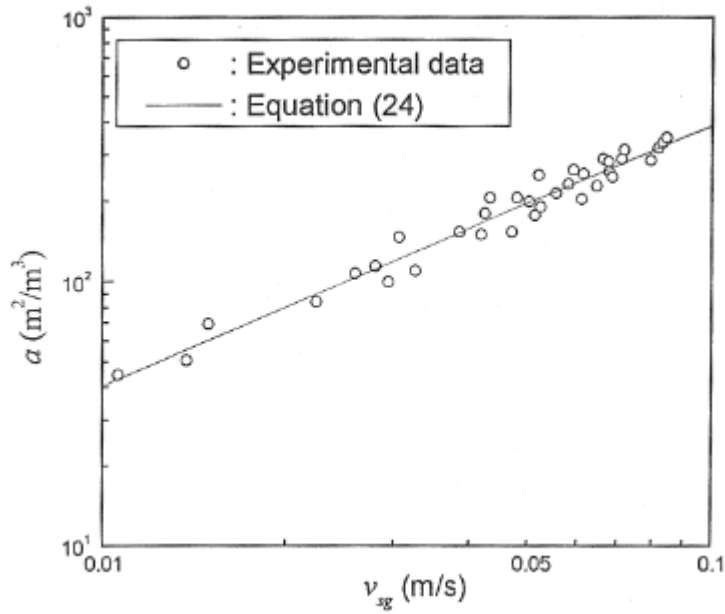


Figure 7 comparison of different experimental values from (Ajay Mandal, 2003) of interfacial area with the values calculated from equation (22)

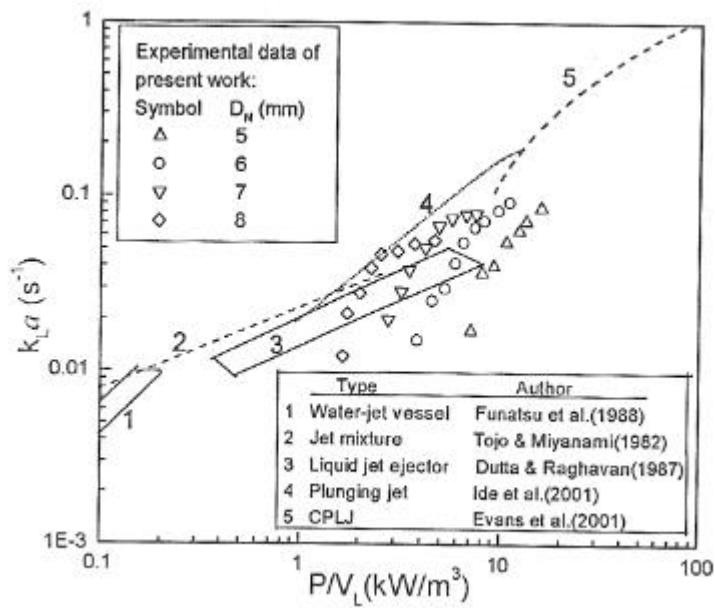


Figure 8 Comparison of $K_L a$ for different gas-liquid contacting devices (Ajay Mandal, 2003)

Figures 8 and 9 can be used to compare with the results of our experiments (Ajay Mandal, 2003).

7 ENHANCEMENT OF MASS TRANSFER FOR SODA-BASED CO₂ CAPTURE

7.1 Bubble size and mass transfer

The absorption of CO₂ is a complex phenomenon in alkaline solutions in which many factors influence the absorption coefficients. The size of bubble affects the mass transfer in a clear way, smaller the bubbles higher the interfacial area and higher the mass transfer. Also when experimenting with gas-liquid separation tanks bubble rise velocity plays a small role in gas-liquid mass transfer, which has a practical value of knowing the residence time in the gas-liquid separation tank as well.

Bedekar determined the properties of sodium carbonate -sodium bicarbonate solutions. Surface tension values were estimated by drop-weight method at different pH and temperatures between 20-25.5°C. It is to be noted that the concentration of the solution was 40.94%. The absorption coefficient and surface tension were very closely related inversely (Bedekar, 1995). The addition of surfactant reduces the surface tension which makes the mass transfer efficient.

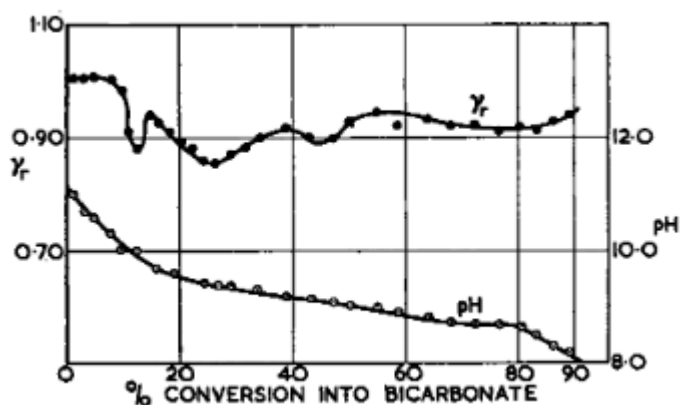


Figure 9 Relationship between relative surface tension, pH and percentage conversion into bicarbonate (Bedekar, 1995)

7.2 Improvement of absorption rate by PPGME

An attempt has been made to improve the absorption rate of the carbonate solution without increasing the absorption capacity of the solution using a surfactant called Polypropylene glycol methyl ether (PPGME) named as DOWFROTH 200 which is non-hazardous. The reason to choose this surfactant is it reduces the gas bubble size distribution and average bubble diameter which in turn increases the gas- liquid interfacial area resulting in a higher absorption rate. The experiment was conducted with 16% CO₂ and remaining air gases in combination. Separate monitors were used to control the CO₂ and air volumetric flowrates, the PPGME concentrations were varied. The difference between the CO₂ fed and CO₂ exhausted (which was calculated by an infrared gas analyser) was taken as the absorption rate. The results

conclude that when increasing the concentration of PPGME, increases the gas- liquid interfacial area and also the absorption rate increases which was accounted for 14% compared to the solution with no PPGME.

It's interesting that the increase of interfacial bubble area by 300% has an impact of only 14% increase in the CO₂ absorption rate. From the above equation it can be predicted that, if the K_L value remained constant then CO₂ absorption rate should also be increased to 300% but here the probable cause for this, could be that the layer of surfactant on the bubble reduces the K_L value by causing lower permeability film over the bubbles surfaces. So higher concentration will also significantly increase the density of this film which can be derived from Gibbs absorption equation (Brett P, 2013), which makes the CO₂ absorption rate inequivalent. The resultant effect would be, by increasing the surfactant concentration would nullify the increase in absorption rate since the increased bubble surface area (Vázquez, et al., 2000) (Vasconcelos, et al., 2002).

The concept of film over the bubbles was well substantiated by comparing two models. The bubble size will impact in determining the gas-liquid interfacial area across which the mass transfer gaseous CO₂ to the bulk phase takes place and also affects bubble rise velocity and gas hold-up (Rodrigo A, et al., 2005). The solution surface tension also holds an important role in determining the bubble size and any change in the bubble size will have effects in velocity and retention time of the bubbles, which will manipulate the buoyancy force of the bubble in solution. This correlation is obtained from the equation (23).

$$F_B = \left(\frac{4\pi}{3}\right)(\rho_L - \rho_G)g - r_b^3 \quad (23)$$

Where F_B - buoyancy force, ρ_L and ρ_G liquid and gas densities respectively, g is the acceleration due to gravity, r_b - bubble radius.

Also in the rising bubble with the surfactants concentrate towards the rear end of the bubble which will add weight resulting in more drag force. In nutshell when the surfactant concentration is increased the bubble rise velocity is decreased and the gas hold up increases, thus giving gas to have longer exposure time to the solution.

However when the PPGME concentration was increased over 0.12g/L the absorption rate diminishes which shows that surfactant inhibits the mass transfer of CO₂ to the bulk liquid phase, to be clearer it impacts the liquid side mass transfer coefficient. The possible causes are

surfactant altering the behaviour of the gas-liquid interface by two ways 1) by creating an immobile interface, 2) by creating a surfactant film around the bubble. The immobile interface will induce poor mixing of the solution at the gas-liquid interface which results in the solution to get saturated with the CO₂ already in contact with the gas bubble and reducing the driving force for CO₂ transport across the interface.

Since the act of diving force keeps itself a primary parameter, it was compared between % change in absorption rate and % change in solution surface tension, which results to be linear. This also indicates that the CO₂ absorption rate in carbonate-based solvents is highly dependent on surface tension of the solution. Plots of different models were used to compare the experimental values with the theoretical values and the inference from the comparisons it is known that the surfactant is creating a film around the bubble and not an immobile gas-liquid interface, so adding more surfactant would create more dense films around the bubble (Spigarelli, 2013).

8 MICROBUBBLE GENERATION DEVICES

Microbubble generation devices have emerged as a most promising option to enhance gas-liquid interfaces in mass transfer. Also in the field of waste water treatment microbubble generation (MBG) devices are of great importance since its boosts the energy efficiency. The primary objective of MBG would be to produce small bubbles with low consumption of energy. These devices are classified mainly into 4 types dissolved air flotation, static mixer, rotary liquid flow and nozzle types depending on the principle of microbubble generation. The advancements in the MBG are based on 3 primary principles 1) pressurization dissolution 2) rotating flow for microbubble generators 3) cavitation for microbubble generators or venturi methods. Some recent upgrades were based on porous media, constant flow nozzles, gas spargers coupled with impellers (Liew, et al., 2020) (Chang HunLee, 2019).

8.1 Venturi type bubble generator

A study of venturi type bubble generator is performed with water and air. The performance of bubble generation, mechanisms dominating the bubble breakup were analyzed. This microbubble generation device produced 0.2-0.4 mm diameters of bubbles approximately. Although the average bubble size depends on liquid Reynolds number and surface tension which suits for straight channels only, for venturi channels the bubble dynamics are different. The bubble breakups in the turbulent flow in straight pipes was investigated and the reasons were 1) turbulent fluctuation and collision, 2) viscous shear stress, 3) interfacial stability, which needs to be considered. The water and air flowrate used in the test was 0.2-1.2L/min and 0.001-

0.16 l/min respectively. A high-speed camera was used to record the bubbles and breakup process and the bubble average diameter was calculated using MATLAB, calculating the Sauter mean diameter. As the liquid flow increases the viscous shear stress increases which plays a major role in bubble breakup. Regarding the average bubble size, as the size of the venturi increases the bubble size is doubled. The primary drawback would be the void fraction, if it is more than 0.1 there would be difficulties in producing microbubbles with venturi type bubble generator (Huang, et al., 2020).

8.2 Oxygen dissolution by venturi-orifice bubble generator

This experiment involves a venturi-orifice type MBG (works on Bernoulli's principle) with water and air conducted at 20°C with the liquid velocity ranging from 35-40 L/min. Sodium sulfite was used to deoxygenize the water (initial concentration of dissolved oxygen 4.0 to 4.5 ppm) and a catalyst was (cobalt chloride) used. The venturi-orifice was fixed with the discharge stream of the submerged pump which has an inlet stream coming from the sides containing various proportions of air and water. The oxygen dissolution effects assessment was done by speculating 3 different effects viz, 1) effect of liquid velocity at constant gas velocity, 2) effect of gas velocity at constant liquid velocity and 3) effect of liquid velocity at free flow of air. $k_L a$ was determined by the data of dissolved oxygen (DO) concentration vs time. The effects of liquid and gas velocities were analyzed and it's interesting to find that the difference in DO increment rate as a function of time can be linked to the liquid velocity in affecting the mixing and distribution of bubble sizes. Since the oxygen peaks were obtained at a liquid velocity of 2.43 m/s and air velocity was constantly maintained at 3L/min, the previous statement stands valid but the velocity of gas (3L/min) makes the bubble size big which decreases the interfacial area thereby leading to lower oxygen dissolution rates. The optimum liquid velocity was concluded as 2.43 m/s which can help to produce bubbles of smaller diameters thereby bubbles having slow rising speed and having plenty of time for oxygen gas to dissolve in water. The relationship of gas and liquid velocity with $k_L a$ was also analyzed and it was deduced from the graphs of air flowrate and $k_L a$ that higher $k_L a$ values were obtained under by increasing the air velocity and maintaining the liquid velocity constant (Liew, et al., 2020).

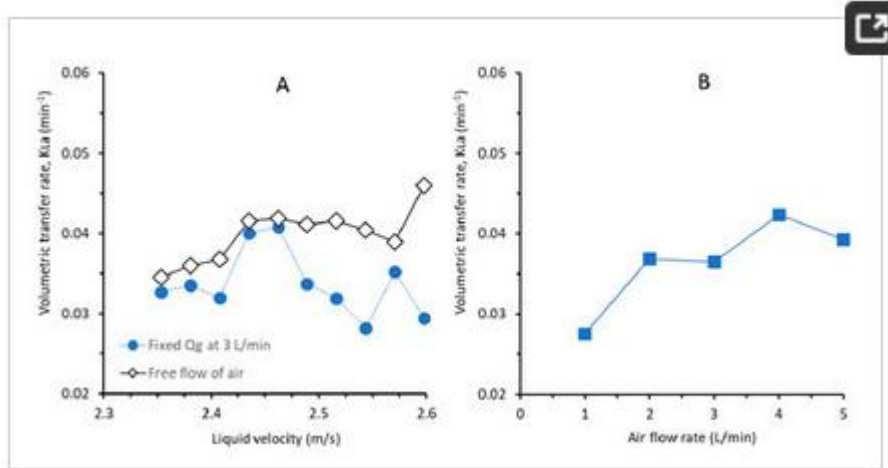


Figure 10 Effect of liquid velocity at fixed air velocity of 3 L/min and under free flowing of air (A) and the effect of air velocity at a constant liquid velocity of 2.46 m/s (B) on the volumetric mass transfer coefficient (Liew, et al., 2020).

EXPERIMENTAL PART

9 DESCRIPTION OF THE CARBON CAPTURE EXPERIMENTS IN THE PILOT UNIT

Experimental part of the thesis is focussed mainly on the mass transfer, efficiency of the whole system, bubble size measurements conducted as a part of VTT's E-Fuel project between April and May and by August 2021. Synthetic gas mixture was tested at pilot unit by absorption-based post combustion capture technology. The tests were conducted by using a new type, high performance microbubble generator developed by VTT (Enhanced Soda Scrubbing process) located at VTT premises in Espoo.

Schedule, content and objectives of the experiment are presented in the table

Table 2 Schedule, objectives of the experiments

Week	Type of gas	Tested methods	Test objectives
#21	Air	Oxygen measurements with water and 8 w-% Na_2CO_3 solution	Estimate CO_2 mass transfer rate with no reaction
#22	Synthetic gas mixture	Mass transfer rate measurements with 8 w-% Na_2CO_3	Estimate CO_2 mass transfer efficiency using recorded pH and vent gas data

		solution using pipe length A and B	
#22	Air and synthetic gas mixture	Images recorded of bubbles using pipe length A and B	Estimate bubble size, mass transfer rate estimation based on bubble size
#33	Synthetic gas mixture	Mass transfer rate measurements by maintaining low liquid level in separation tank	Estimate CO ₂ mass transfer efficiency using recorded pH and vent gas data
#34	Synthetic gas mixture	Mass transfer rate measurements by placing the microbubble generator in vertical position and images recorded of bubbles using length A and B	Estimate CO ₂ mass transfer efficiency using recorded pH and vent gas data, determine the bubble size and mass transfer based on bubble size

The experiments were conducted by using capture equipment built inside shipping container, which ensures the safe mobility of the equipment. The tested methods are more specifically explained below.



Figure 11 The experiments were conducted at the VTT's enhanced soda scrubbing process mobile unit

9.1 Data Processing

Test data from the experiments was processed manually. To smoothen the process of data processing some individual test runs whichever needed were drawn into graphs. To equate the recorded measurement time intervals of different parameters MS Excel was used. For example, the CO₂ lean gas out from gas-liquid separation tank data was logged in a time interval of 5 seconds, for the same experiments the pH was logged for every one minute.

For oxygen measurements the length of the test period varied from 5 to 15 min depending on the L/G ratio, for the mass transfer rate measurements test period varied from 5 to 10 min. Test periods for bubbles size measurements were approximately 10 to 15 min for each frame focussed.

9.2 Dissolved oxygen measurements

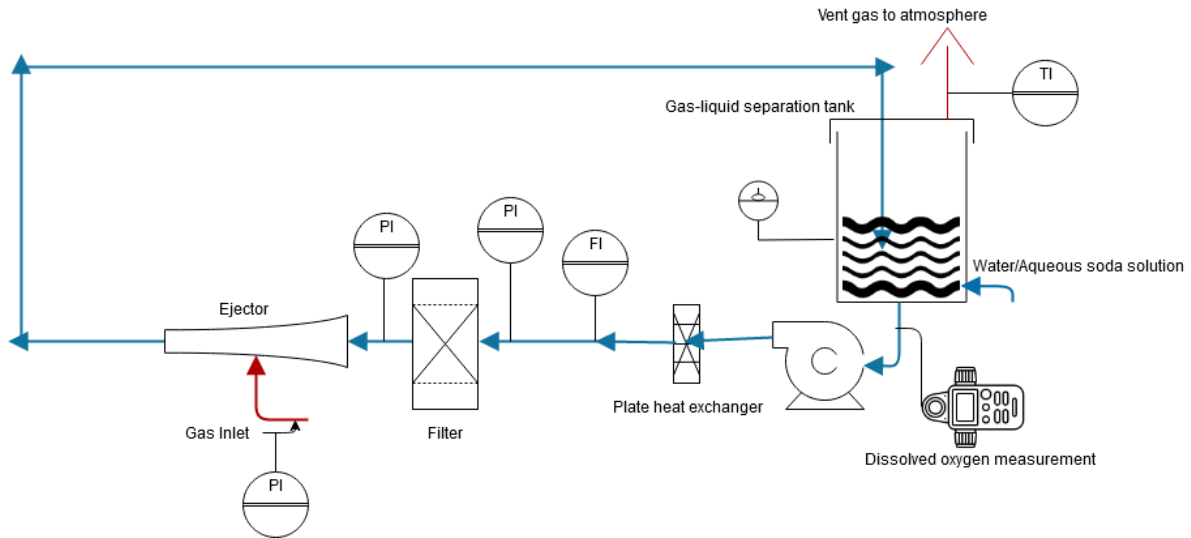


Figure 12 A schematic flow diagram of oxygen measurement setup

The background aim behind this experiment is to estimate the mass transfer rate of the system with no reaction happening, Figure 12 which represents a schematic flow diagram of the process. The system is filled with water, with the help of a portable diaphragm pump which will be temporarily attached to the vent pipeline of the gas-liquid separation tank. The liquid filling line of the separation tank is dipped into the solution and the pump attached to the other end of the gas-liquid separation tank starts to produce vacuum. When the liquid level reaches $\frac{1}{4}$ height of the separation tank which is monitored from the sight glass, the circulation pump is switched on so that gas in the system is also removed, this process is continued until the desirable liquid height is reached in the gas-liquid separation tank. From the level of the liquid which is left in the container, the volume of the liquid in the system is noted.

The circulation pump frequency is adjusted to get the desirable flowrate which is measured by a rotameter located after the circulation pump. The system is unaerated by introducing pure nitrogen gas into the system which removes the oxygen by bubbling out. The process of mixing happens in the microbubble generator, which is similar to a nozzle type equipment, contains a shaft at the centre which has carved vanes. While the liquid is in circulation the carved vanes produce swirls in the liquid and the gas which enters from the side of the microbubble generator which passes through a perforated metal sheet produces small bubbles and the swirls produced from the vanes dissolves the gas bubbles efficiently.

An oxygen probe situated at point A (after separation tank), Point B (after microbubble generator), which is connected to the YSI pro ODO dissolved oxygen measurement device manufactured by Xylem Analytics Ltd., (YSI, 2020) measures and logs the data which is later retrieved from KorrDss Data manager software (YSI, 2021). The dissolved oxygen is measured after separation tank (Point A), measured. The experiment is started only after ensuring the dissolved oxygen concentration is nil in the circulating liquid in the system. The mass flow controller units manufactured by Environics Ltd., is used to monitor the inlet gas composition. Soon when the oxygen concentration is zero the nitrogen is stopped, air valve is turned on and stopped when the oxygen concentration fails to increase further in the circulating liquid. The L/G ratio tested were 1, 1.5, 0.75, 1.25. After each test runs the system is unaerated to the maximum. The same experimental procedure was tested for 8 w-% Na₂CO₃ solution and air. To check the effect of inlet pressure of the liquid on DO concentration was experimented by tuning the gap with a screw between the gas and liquid in the microbubble generator.

These experiments were carried out in week #21. The dissolved oxygen concentrations were logged after the gas-liquid separation tank for water and air, 8 w-% Na₂CO₃ and air. Different L/G ratio was used as mentioned in section 7.1 and the liquid, gas pressure varied from 0.3 to 0.95 bar. Time lag measurements were performed using a gas impinger before the dissolved oxygen probe is used for experiments, represented by Figure 13. Approximately 150 ml of water is filled in the gas impingers and the nitrogen is flushed for some time to get the water unaerated through a glass tube which reaches till the bottom of the impinger and bubbles out the oxygen present in the water. The oxygen probe is then inserted into the impinger and the time it takes to reach 63.21 mg/L concentration will be the time lag or response time of the probe, represented by Figure 14. It is because, in our case oxygen is transferred from gas to liquid. So, the flux would be

$$N = K_L a (C^* - C_L) \quad (24)$$

Solving for liquid side oxygen concentration, C_L

$$C_L(t) = C^* (1 - e^{-K_L a t}) \quad (25)$$

Integrating, when $C_L = C^* (t)$

$$C_L = C^* (1 - \frac{1}{e}) \quad (26)$$

$$\frac{C_L}{C^*} = 1 - \frac{1}{e} = 0.6321 \quad (27)$$



Figure 13 Gas impingers used in time lag measurements for DO

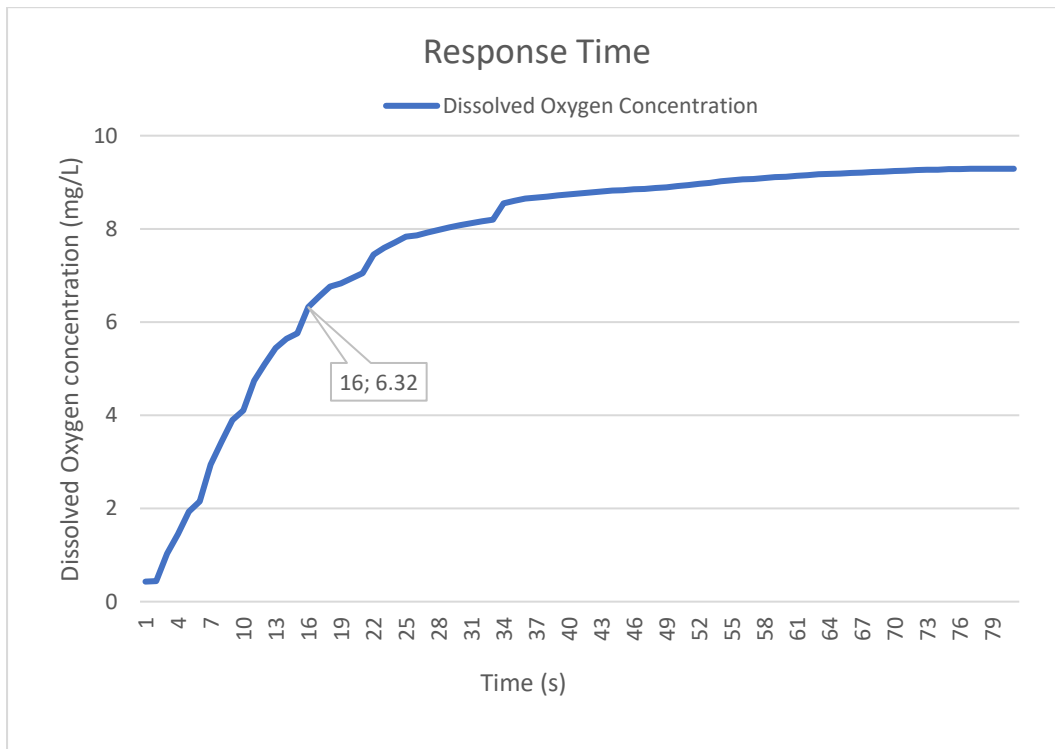


Figure 14 Time lag measurement for DO probe

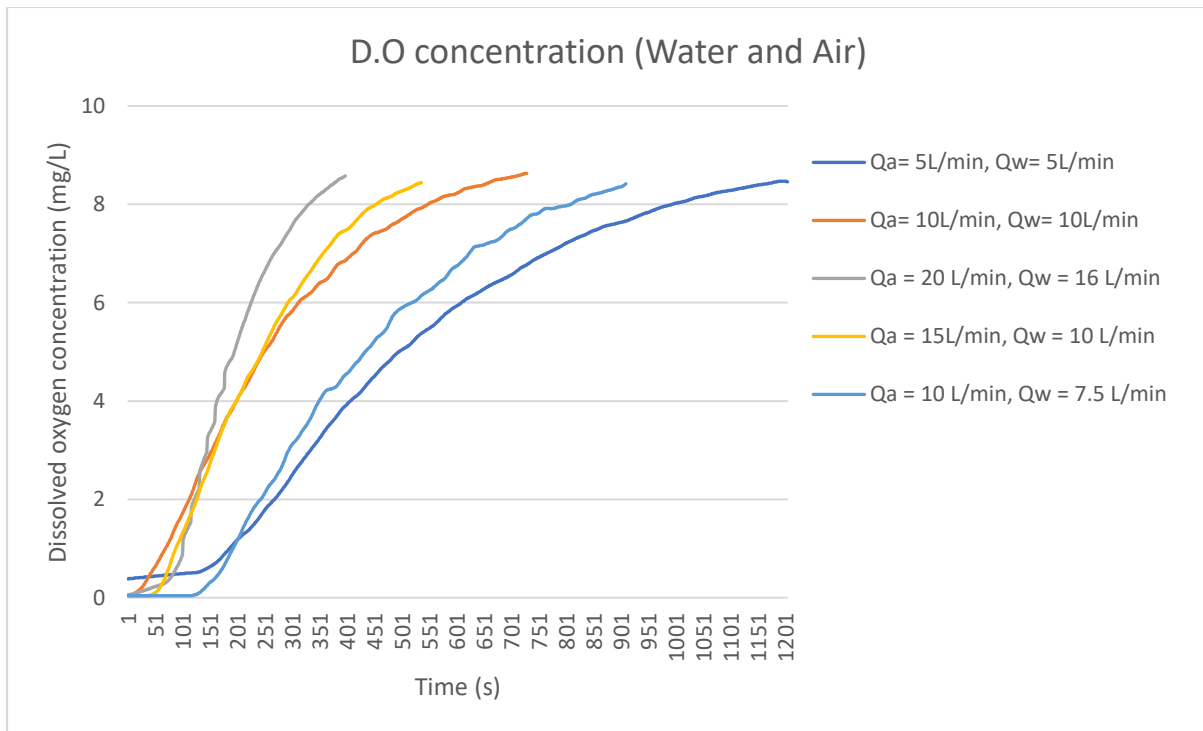


Figure 15 Dissolved oxygen concentration measured at point A

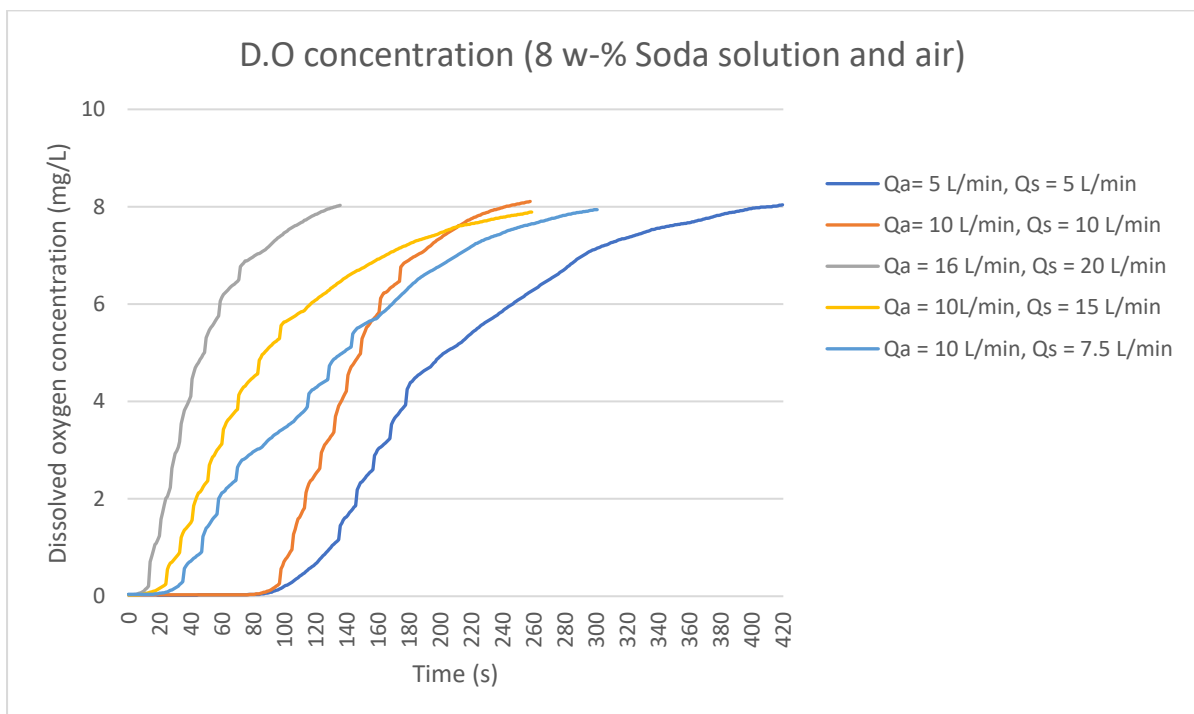


Figure 16 D.O concentration (8 w-% Soda solution and air) at point A

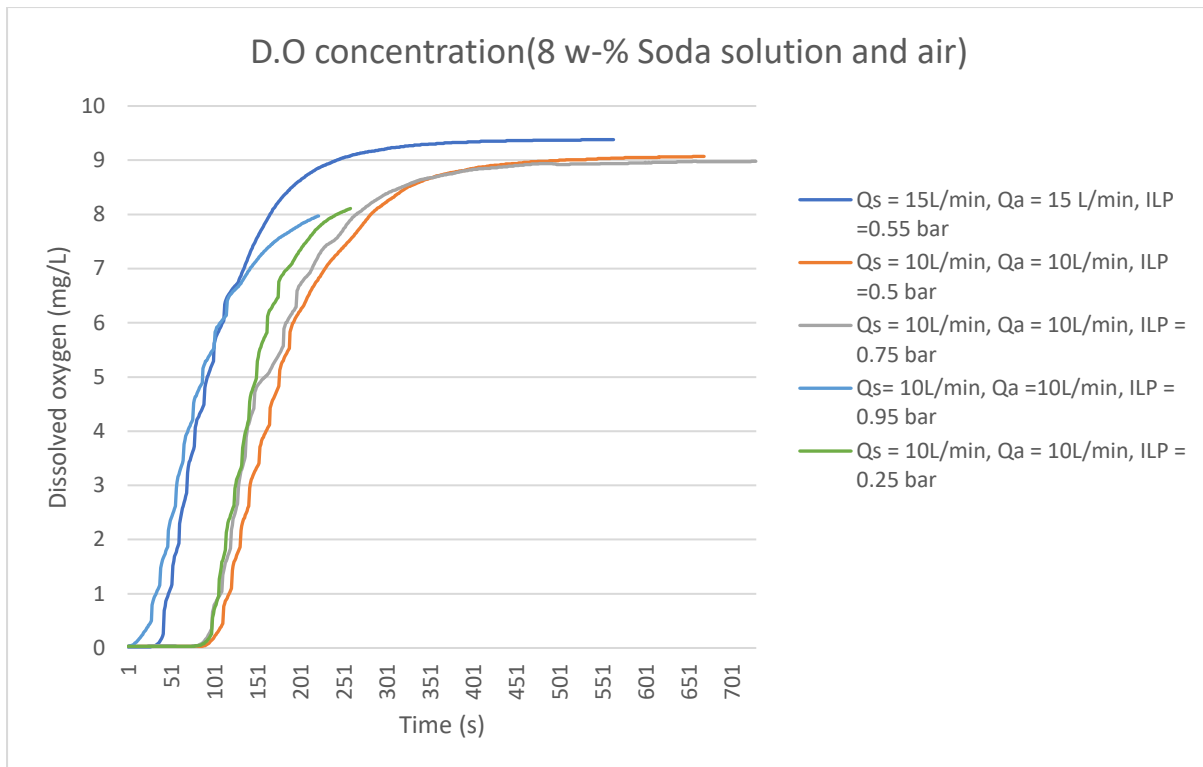


Figure 17 Effect of inlet liquid pressure on D.O concentration measured at point A

The DO concentration measured at point B (after microbubble generator) was highly influenced by the gas which makes it unreliable for calculations. In Figure 14, which depicts the response time of the DO probe which is used in the MATLAB model. Figure 15 and 16 represents DO concentration measured at point A, when comparing figure 15 and 16 it is inferred that oxygen absorption rate is more for 8 w-% soda solution than for water. Figure 17 represents the effect of inlet liquid pressure variation created by tuning the screw of the bubble producing device, higher absorption rates can be achieved which also shows the performance of the tested bubble producing device.

9.3 Results - Mass transfer rate estimation for dissolved oxygen measurement

It is very crucial that we need to know a relationship between the gas phase and liquid phase equilibrium oxygen concentration to predict how quickly oxygen is transported. Considering transfer of oxygen from air into water, the process of dissolution is accelerated by agitation which is more or less similar with the effect of microbubble generator and resulting in decrease of film thickness, hence increase in concentration gradient.

In our case the dynamic measurements obtained from the DO probe contains a time lag within the original oxygen concentration at a time and the probe reading. To investigate further, data

fitting was necessary to estimate the oxygen dynamics. The movement of bubbles in the solution changes its concentration over distance and time, oxygenation capacity of the reactor which is characterized by the gas-liquid volumetric mass transfer and should not be prejudiced by the influence of gas concentration in the bubbles. Hence $K_L a$ modelling was crucial.

A continuous loop reactor (CLR) was assumed to a similar plug flow reactor according to our experimental setup described by mathematical equations (28) and (29) which is acquired from the mass balance.

$$\frac{d}{dt} C_g = -\frac{Q_g}{\varepsilon_g S} \frac{d}{dx} C_g - \frac{k_L a (C_g - C_L)}{\varepsilon_g S} \quad (28)$$

$$\frac{d}{dt} C_L = \frac{Q_L}{(1-\varepsilon_g)S} \frac{d}{dx} C_L + \frac{k_L a (C_g - C_L)}{(1-\varepsilon_g)S} \quad (29)$$

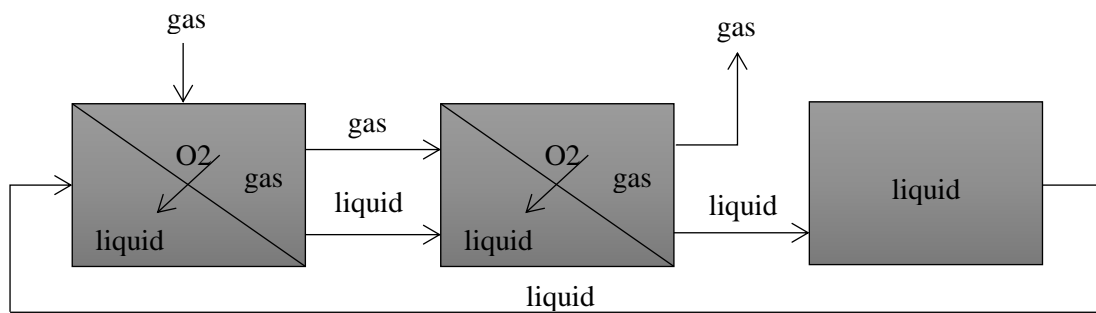


Figure 18 simplified flow of a CLR

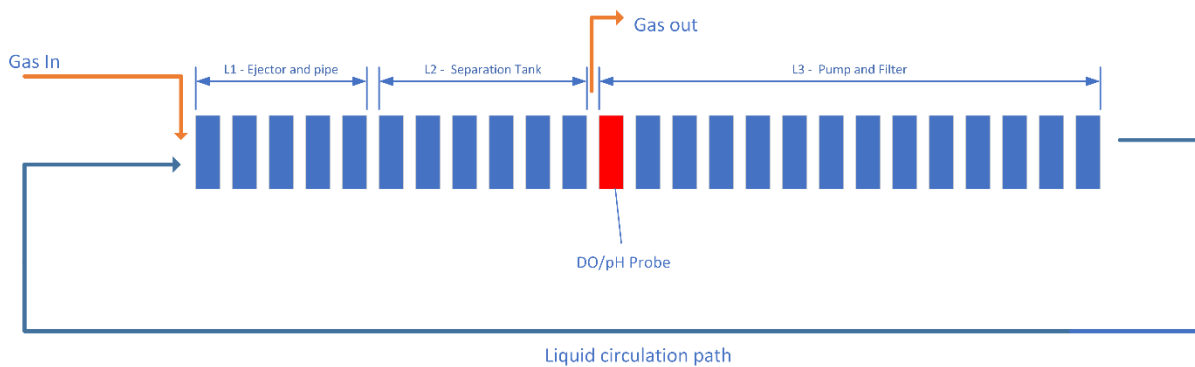


Figure 19 Illustration of a plug flow model in a CLR

Figures 18 and 19 demonstrate the method of PFR modelling as a CLR. The obtained results are represented below in Figures 20, 21, 22 and 23 for different L/G ratio.

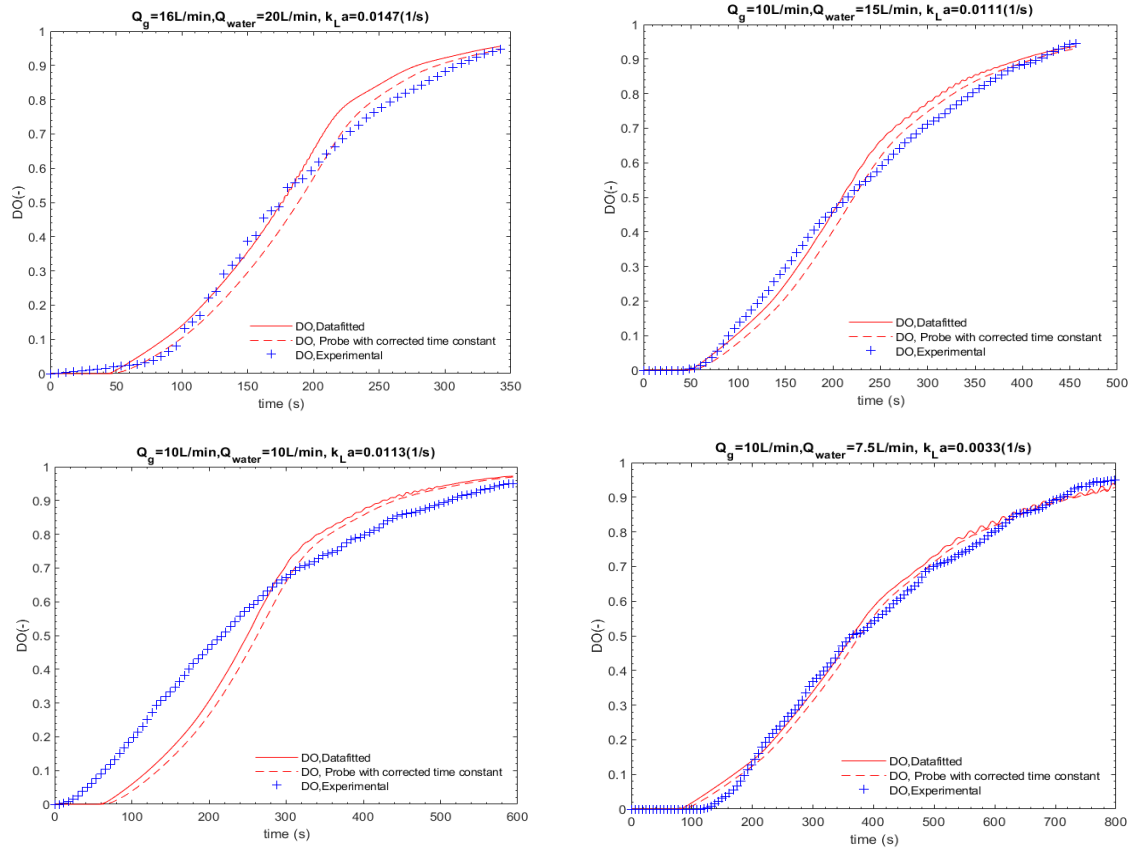


Figure 20 Data fitted plots for water and air

In Figures 20, 21, 22 and 23 the blue '+' signs indicate the experimental readings measured and logged from DO probe which contains the time lag. The red lines (dashed) represent the DO readings with corrected time constant, red line (continuous) represent the model, so in the model the red lines (dashed) is data fitted to the model. The process of modelling is extensively described in Appendix 1.1. It can also be seen that mass transfer rate (without reaction) is quite high for the same L/G ratio for 8 w-% soda solution than for water. The highest mass transfer rate achieved was 0.342 for L/G ratio of 1.25.

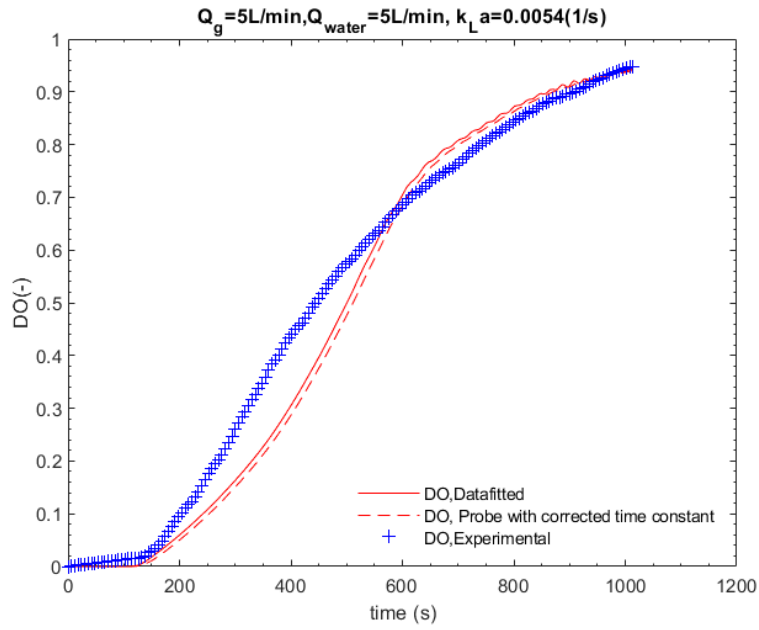


Figure 21 Data fitted plots for water and air

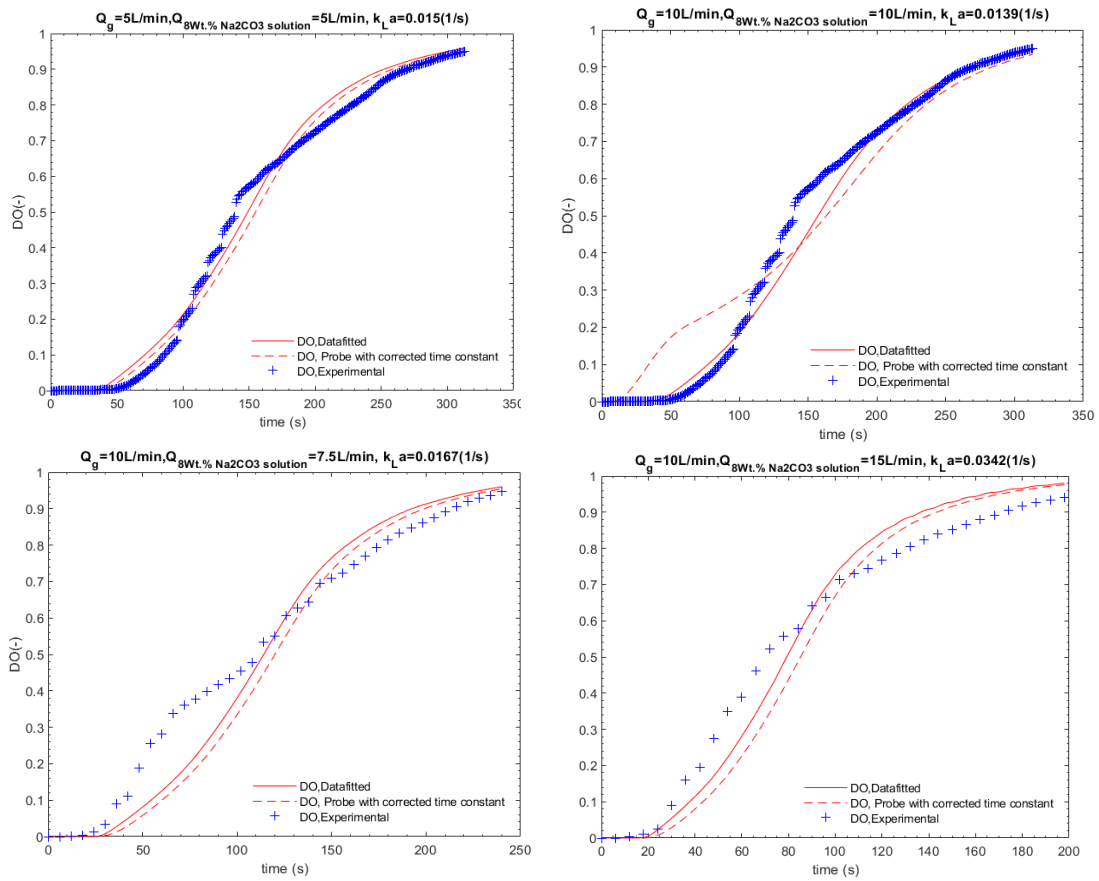


Figure 22 Data fitted plots for 8 w-% Soda solution and air

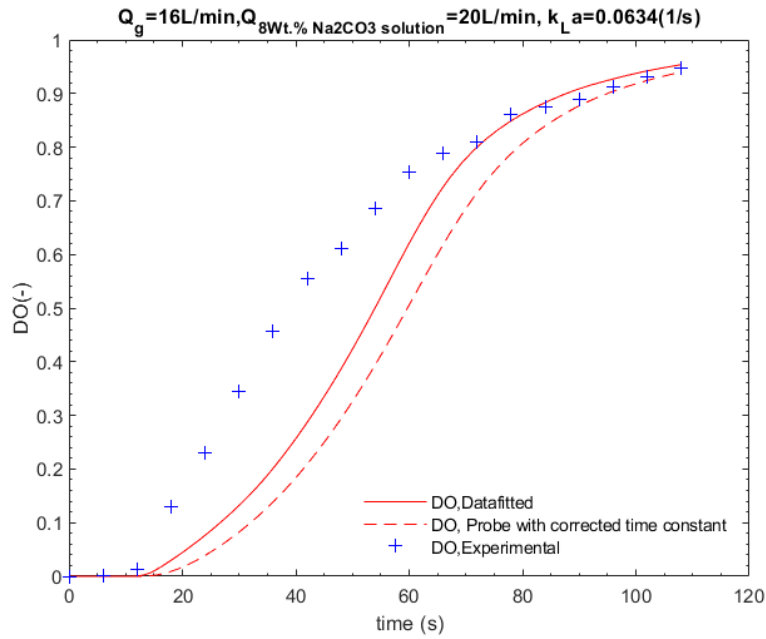


Figure 23 Data fitted plots for 8 w-% Soda solution and air

9.4 Description of Mass transfer rate estimation from CO_2 and 8 w-% Na_2CO_3 experiments

The pH sensors were installed after the microbubble generator and also after the separation tank to check the hydrogen ion activity in the solution. Absorption of synthetic gas mixture (15 vol-% CO_2 + 85 vol-% N_2) in 8 w-% Na_2CO_3 solution was tested and the pH were recorded by using pH sensor S401 manufactured by Chemitec Ltd., for different L/G ratios as same mentioned in section 9.2. The Figure 24 which represents a schematic flow diagram of the experimental setup where there is an interchangeable pipe of two different lengths, pipe A is 10 cm long and pipe B is 100 cm long.

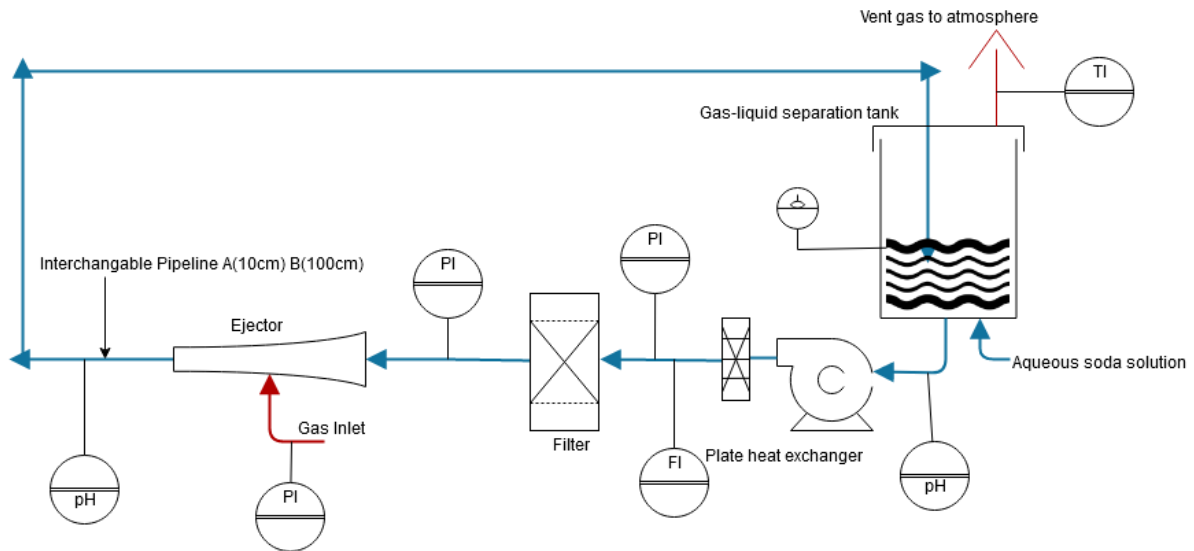


Figure 24 Schematic flow diagram of mass transfer rate estimation

The reason for testing two different lengths was to get an idea about the overall system efficiency and to compare the results. In the gas-liquid separation tank the pipe containing the soda solution and the synthetic gas mixture from the microbubble generator is immersed into the soda solution, so that the gas bubbles manage to escape rising through the liquid to the atmosphere. The inlet gas and liquid pressure varied from 0.05 to 1.00 bar depending on the L/G ratio. The vent gas was analysed by Sidor Maihak gas analyser manufactured by Sick Ltd and logged. A plate heat exchanger was used to increase the temperature of the liquid to 30°C so that it is more pertinent to industrial scale operation and thus substantially reducing the heat duty. When the interchangeable pipe is changed, fresh soda solution is prepared and used for the experiments. Two other experimental setup were also tested for the same L/ G ratio. The soda solution level in the gas-liquid separation tank was maintained low and only pipe A was used, in another setup the microbubble generator was positioned vertically and pipe A was used which is represented in Figure 25.

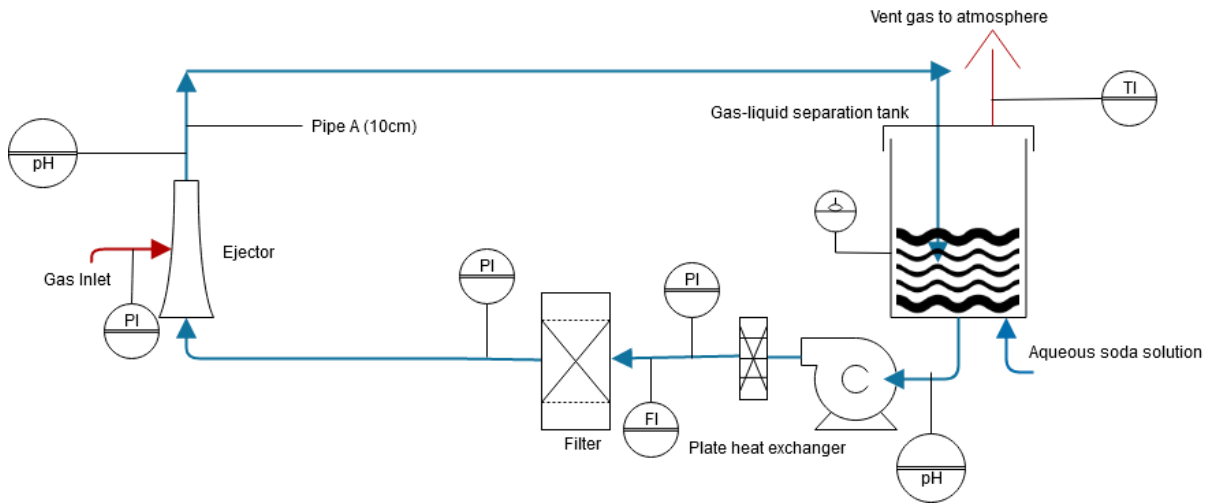


Figure 25 Schematic flow diagram of mass transfer rate estimation in vertical microbubble generator setup

9.5 Results - Mass transfer rate estimation from CO_2 and 8 w-% Na_2CO_3 experiments

As discussed in the section 9.4 the capture rate of CO_2 is obtained for interchangeable pipe A and B, low liquid level in the separation tank, vertically mounted microbubble generator position. The results are presented below in the table.

9.5.1 Mass Balance, Residence Time and CO_2 capture rates

Mass balance for all of the experiments combined is represented by Table 4 and Table 5 represents mass balance of the experiments with same pH range after the gas-liquid separation tank.

Table 3 Mass balance for all the experiments

Scenarios	CO_2 in (g)	CO_2 out (g)	Run time(mi n)	Capture efficiency (%)	pH range after gas-liquid separation tank	pH range after microbubble generator
Pipe A	571.3	44.8	149	92.2	11.4 - 9.76	11.1-9.48
Pipe B	636.3	86.4	191	86.4	10.4 - 9.37	10.4 - 9.08
Low liquid level in gas-liquid separation tank	656.8	135.2	164	79.4	11.2 - 9.03	10.8 - 8.41
Vertically mounted microbubble generator	214.7	0.9	69	99.6	11.6 - 10.3	11.1 - 9.86

Table 4 Mass balance for specific pH range

Scenarios	CO_2 in (g)	CO_2 out (g)	Run time(min)	Capture efficiency (%)	pH range after gas-liquid separation tank	pH range after microbubble generator
Pipe A	396.8	43.1	120	89.1	10.4 - 9.76	10.2 - 9.48
Pipe B	381.4	34.7	111	90.9	10.4 - 9.76	10.4 - 9.56
Low liquid level gas-liquid separation tank	220.6	26.2	62	88.1	10.4 - 9.76	9.93 - 9.16
Vertical microbubble generator	40.2	0.26	17	99.4	10.4 - 10.23	10.00 - 9.86

Table 5 Residence time for the equipment for different L/G ratio

Q_{gas} (L/min)	Q_{liquid} (L/min)	Residence time in the separation tank (s)	Residence time after microbubble generator (s)- using pipe A	Residence time after microbubble generator (s)- Using pipe B
10	15	57.3	5.6	7.6
15	15	47.7	4.7	6.3
10	10	71.6	7.0	9.5
5	5	143.2	14.1	19.0

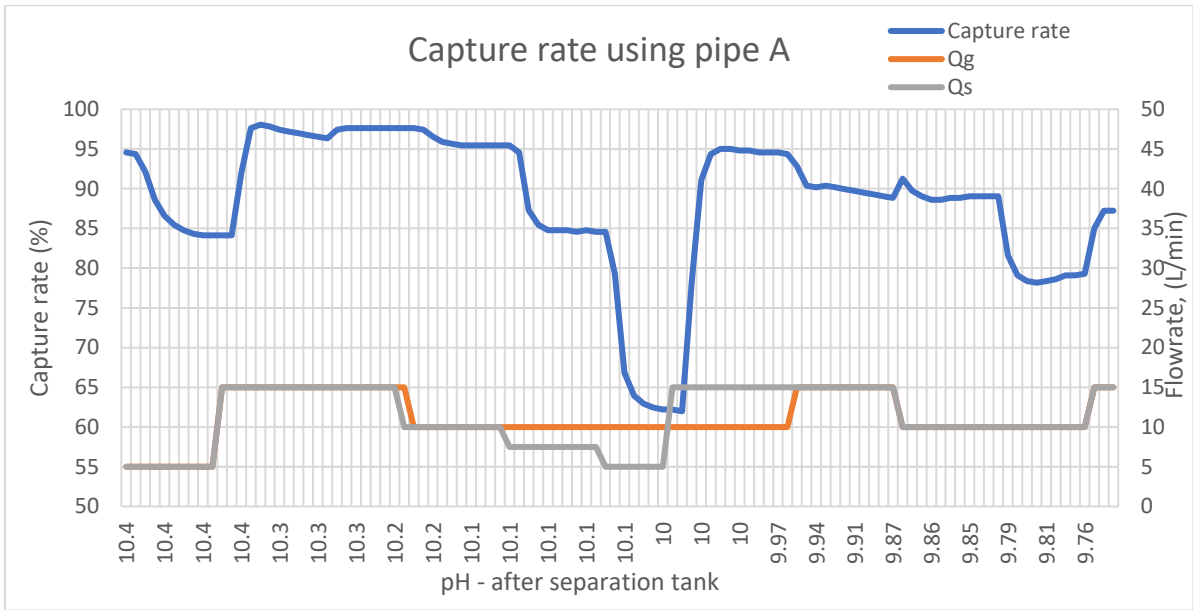


Figure 26 Capture rate using pipe A

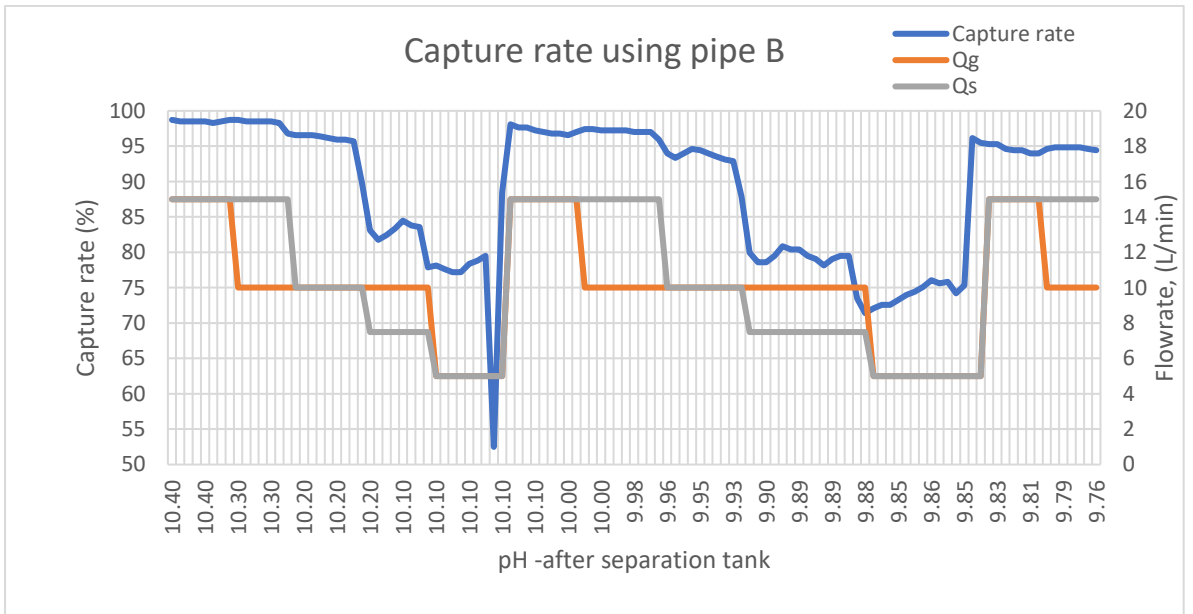


Figure 27 Capture rate using pipe B

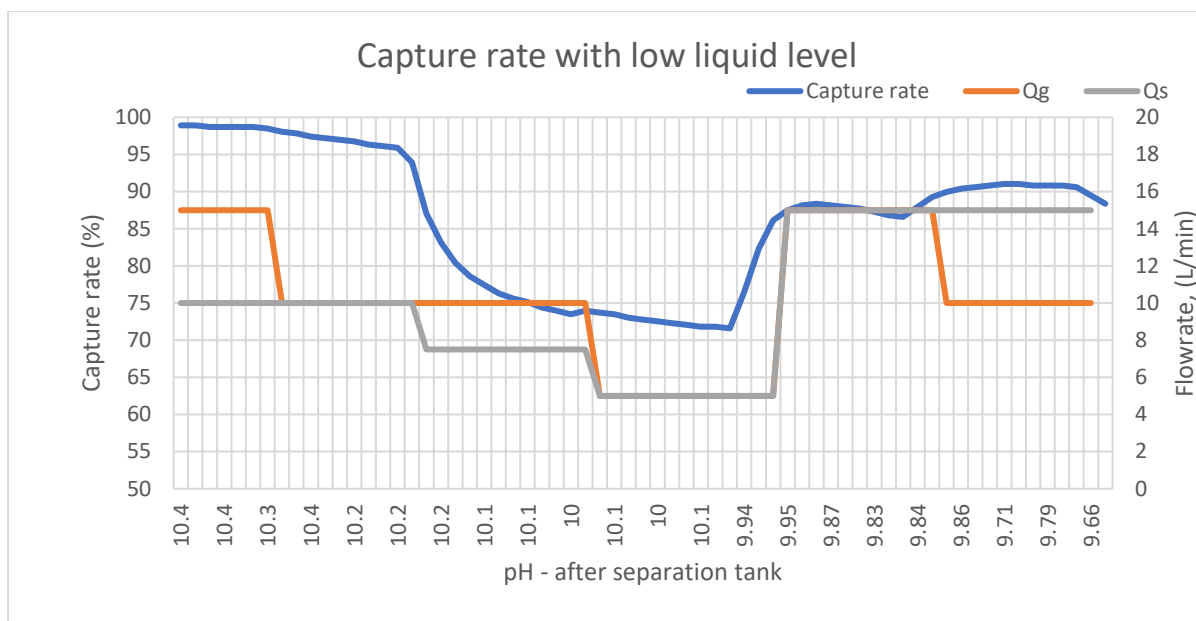


Figure 28 Capture rate by maintaining low liquid level in the gas-liquid separation tank

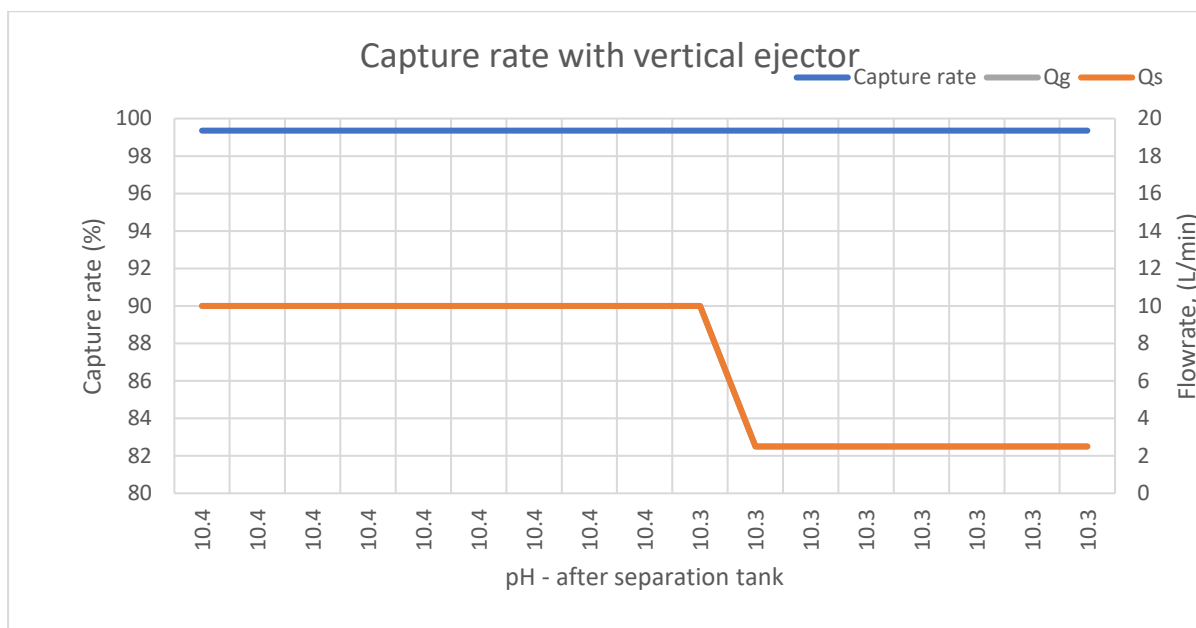


Figure 29 capture rate with vertical microbubble generator setup

The calculation methodology and procedure of estimation of mass transfer rate, capture rate and conditions are explained in detailed in Appendix 1.2.

9.5.2 Reaction kinetic conditions

In the overall reaction, Equation (2) CO_2 is converted to bicarbonate. For this reaction to take place the CO_2 is needed to be absorbed as mentioned in Equation (3) and (4), to be absorbed there are two resistances namely gas phase boundary layer and liquid phase boundary layer, since the reaction (4) is ionic it takes place much faster than Equation (3), which means the first reaction step is rate controlling, Equation (3).

“A diffusion controlled slow reaction is suitable for determining the liquid volumetric mass transfer coefficient, $k_L a$. The absorption of CO_2 into a carbonate-bicarbonate buffer solution is a convenient system” (Ajay Mandal, 2003)

The conditions to check for which the reaction (3) is sufficiently fast so that the CO_2 concentration in the bulk is close to null, which is represented in Equation (30)

$$k_L a \ll \alpha_L K_2 C_B^0 \quad (30)$$

$$\left[\frac{D_A K_2 C_B^0}{k_L^2} \right] \ll 1 \quad (31)$$

Further to check whether the appreciable amount of reaction happens in diffusion films and the condition to verify is represented in Equation (31).

Table 6 Equation (30) verification with experimental data

pH range after gas-liquid separation tank	$k_L a$ (cm/s m)	$\alpha_L K_2 C_B^0$
11.6 - 8.99	12.18 - 39.899	7.68×10^{11}

In Table 7 the $k_L a$ values calculated using condition (30) is in the range 12.18 - 39.899 for pH between 11.6 - 8.99. It is to be noted that the value of $\alpha_L K_2 C_B^0$ is not less than $k_L a$ value, which means the reaction is sufficiently fast and CO_2 concentration in the bulk of the liquid is close to zero.

Table 7 Equation (31) verification with experimental data

pH range after gas-liquid separation tank	$\left[\frac{D_A K_2 C_B^0}{k_L^2} \right] \ll 1$
11.6 - 8.99	9.7405×10^5 to 1.23×10^6

The inference from Table 8 is that for the pH range of 11.6 - 8.99 in our experiments the value of $\left[\frac{D_A K_2 C_B^0}{k_L^2}\right]$ is much higher than 1 which indicates that appreciable amount of reaction happens in liquid films.

9.5.3 Enhancement Factor

Enhancement factor, E which estimates how many times the reaction is faster with chemical reaction than without chemical reaction ($k_L a$ obtained from dissolved oxygen measurement using 8w-% Na_2CO_3 solution). Essentially it is the ratio between mass transfer rate coefficient with reaction to the mass transfer coefficient without reaction. For a reversible reaction to which the rates are defined, it is very crucial to know the reaction kinetics when interpreting the gas-liquid interface mass transfer. To get a deeper idea about the performance of a given solvent, one should understand the phenomena of jumbled mass transfer as well as the enhancement due to chemical reaction for mass transfer. The R^2 values represented in Table 9 gives an idea about the data fit goodness in MATLAB model. The calculation procedure of Enhancement factor is explained in Appendix 1.4

Table 8 Enhancement factor using pipe A

Scenario	with pipe A						
Q_{gas} (L/min)	Q_{liquid} (L/min)	Liquid mass transfer rate with reaction (1/s)	Liquid mass transfer rate without reaction (1/s)	Enhancement factor, E	pH-after microbubble generator	R^2 values (air and water)	
5	5	0.13	0.015	8.6	10.19	0.95	
10	10	0.24	0.0139	17.3	10.41	0.64	
10	7.5	0.15	0.0167	9	10.25	0.86	
10	15	0.8	0.0342	23.4	10.65	0.80	
10	10	0.11	0.0139	8	9.6	0.64	
10	7.5	0.11	0.0167	6.6	9.53	0.86	
10	15	0.3	0.0342	8.7	9.77	0.80	

Table 9 Enhancement factor using pipe B

Scenario	with pipe B				
Q_{gas} (L/min)	Q_{liquid} (L/min)	Liquid mass transfer rate with reaction (1/s)	Liquid mass transfer rate without reaction (1/s)	Enhancement factor, E	pH-after microbubble generator
5	5	0.19	0.015	12.6	10.03
10	10	0.19	0.0139	13.6	10.21
10	7.5	0.21	0.0167	12.6	10.11
10	15	0.5	0.0342	14.6	10.26
5	5	0.08	0.015	5.3	9.39

Table 10 Enhancement factor by mounting microbubble generator vertically

Scenario	vertical microbubble generator					
Q_{gas} (L/min)	Q_{liquid} (L/min)	Liquid mass transfer rate with reaction (1/s)	Liquid mass transfer rate without reaction (1/s)	Enhancement factor, E	pH-after microbubble generator	Superficial gas velocity, (m/s)
5	5	0.15	0.015	10	11.1	0.092
10	10	0.15	0.0139	10.7	10	0.184
10	7.5	0.14	0.0167	8.3	10.7	0.184
10	15	0.53	0.0342	15.4	10.1	0.184

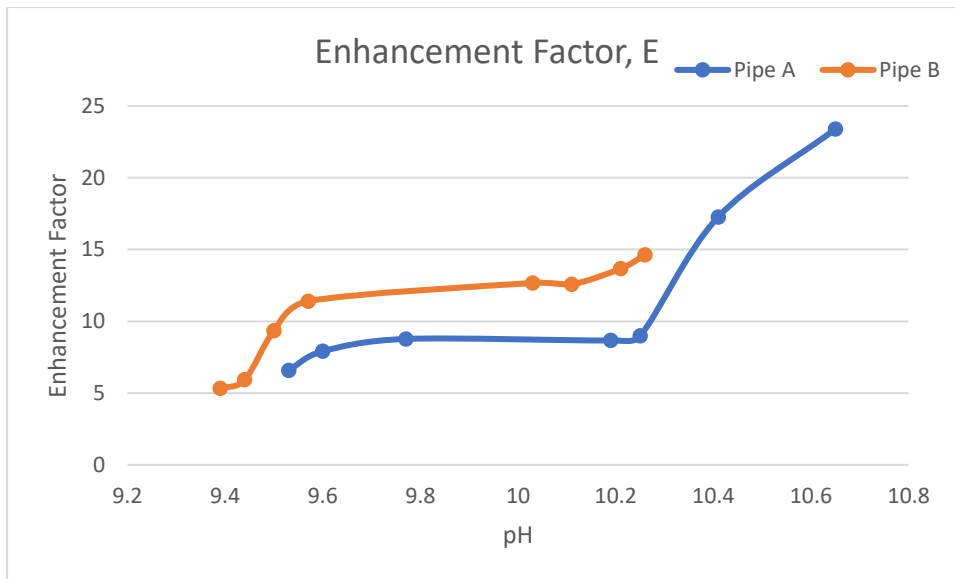


Figure 30 Enhancement factor for the experiment performed with interchangeable pipe A and B

Mass transfer enhancement due to chemical reaction happens according to the pH of the solution. pH is a function of L/G ratio, higher the L/G ratio quicker the pH decreases. It is also important to know that good interfacial area is necessary for effective mass transfer which is limited by bubble agglomeration. In pipe B bubble agglomeration is high and therefore the mass transfer enhancement would be lower when compare to pipe A

9.6 Description of the bubble size measurements

The bubble size estimations were necessary to compare the interfacial area under different flow conditions. A transparent pipe of 34 mm internal diameter was attached to the end of interchangeable pipelines. To avoid the optical distortions caused by circumferential surface of the transparent pipe, it was placed in a perplex container filled with water, which was highly helpful in studying the bubbles. A high-speed camera FASTCAM SA-Z type 2100K, manufactured by Photron Deutschland GmbH, Reutlingen, Germany was used to record the images, represented in Figure 32. A white mate sheet was fixed at the back side of the perplex box to nullify the reflections from the background. Two halogen lamps and slit were used for lighting purposes. A ruler was fixed at the top of the transparent pipe to differentiate the focus area. The frame rate was varied from 3000 to 10000 frames per second depending on the intensity of bubbles. Shutter speed was varied accordingly depending on the stream flow rates to avoid motion blur. The focal distance was 30 mm to a corresponding maximum of 1.7 cm depth from the pipeline walls and captured 600-1000 frames per measurement.

The same setup was used to record images for both interchangeable pipe A and B (Figure 32 left) and for vertical microbubble generator setup only with pipe A, represented in Figure 33.

In the transparent pipe the images were recorded at 3 points along the flow, shown in Figure 31

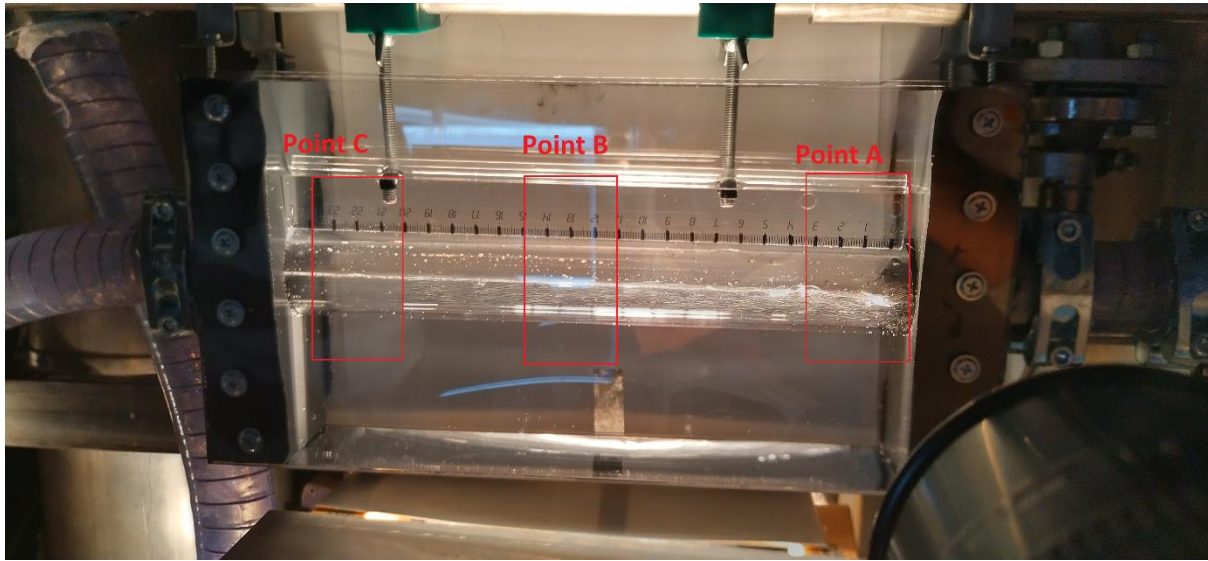


Figure 31 Recorded image frame focal locations

The recorded images were analysed using PFV Version 3691 software and the bubble size were estimated for comparison.

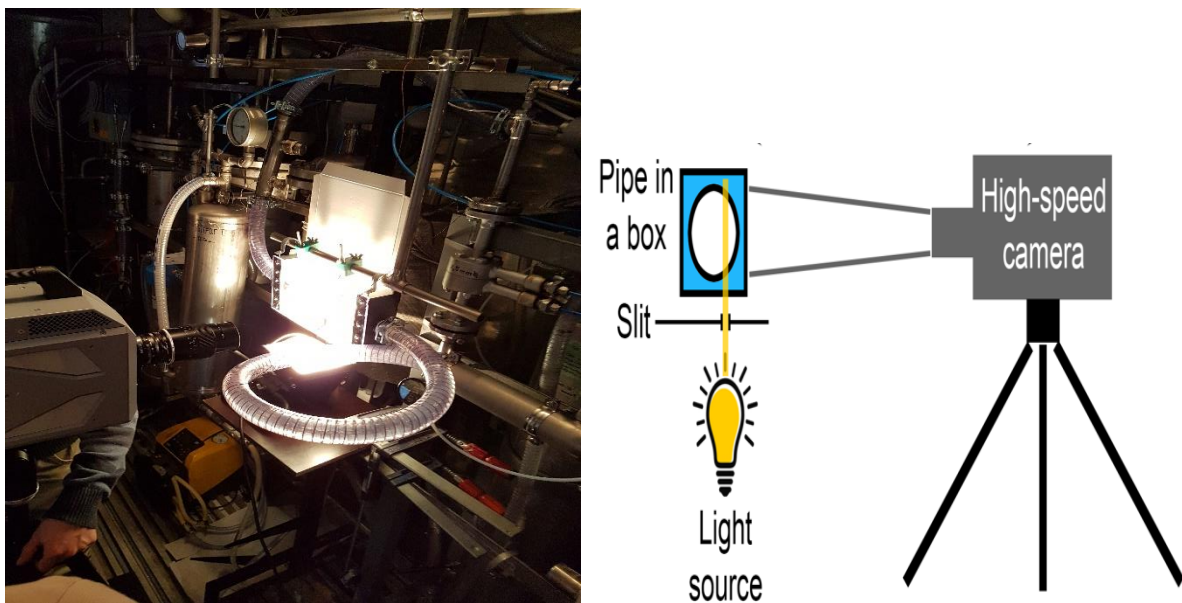


Figure 32 High speed camera setup (left), schematic representation of camera focal plane location side view (right)

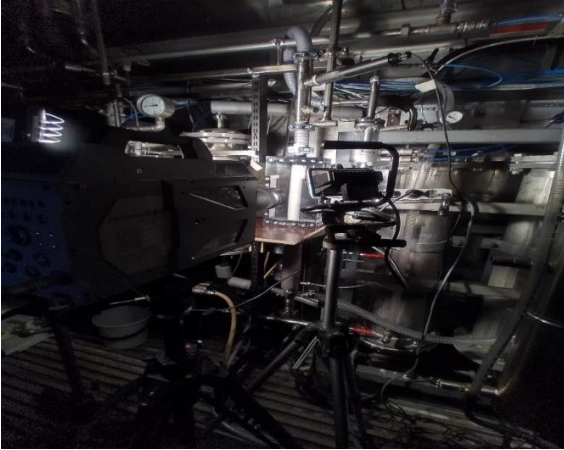


Figure 33 High speed camera setup with ejector positioned vertically

9.7 Results – Bubble size measurements

Various L/G ratios and using pipe A and pipe B, microbubble generator mounted vertically was recorded by high-speed camera and the images were analysed, flow inside the tube was studied, calculating the liquid phase mass transfer coefficients (k_L) from dimension less numbers are represented below in table 10 and 11. Since the k_L value is calculated from the average bubble diameter the influence of average bubble diameter is high in the k_L value and so it is a rough estimation to have an idea. By following the individual bubbles local bubble velocity was also estimated. The flow regimes for two phase flow in a horizontal pipe was also compared.

Table 11 Average bubble diameter for air and water

Flow rate, (L/min)		Average bubble diameter(μm)	k_L , (m/s)	Reynolds Number(water)	Superficial gas velocity, (m/s)
Q_{air}	Q_{water}				
5	5	4140	2.1×10^{-3}	3.51×10^3	0.092
10	10	4250	2.19×10^{-3}	7.1×10^3	0.184
10	7.5	440	1.35×10^{-3}	5.26×10^3	0.184
10	15	370	2.01×10^{-2}	1.05×10^4	0.184
16	20	368	2.70×10^{-2}	1.12×10^4	0.293

Table 12 Average bubble diameter for air and 8w-% Na₂CO₃ solution

Flow rate, (L/min)		Average bubble diameter, (μm)	k_L , (m/s)	Reynolds Number (8w- % Na ₂ CO ₃ solution)
Q_{CO_2}	$Q_{8w-\%Na_2CO_3}$ solution			
5	5	2500	9.30×10^{-3}	3.40×10^3
10	10	2580	2.74×10^{-2}	6.79×10^3
10	7.5	398	1.13×10^{-2}	5.09×10^3
10	15	334	4.32×10^{-2}	1.02×10^4

9.7.1 Dissolved Oxygen measurements

As mentioned in section 7.3 the images were recorded at 3 points. Figure 32 represents the

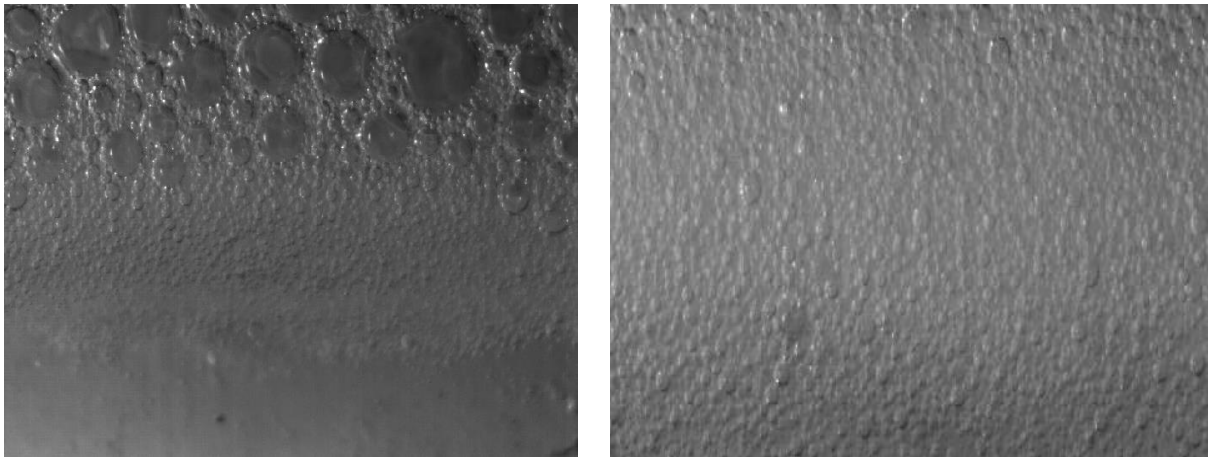


Figure 34 Oxygen bubbles dispersed in water recorded at point A (surface of the pipe), L/G ratio 1(left), L/G ratio 1.25(right)

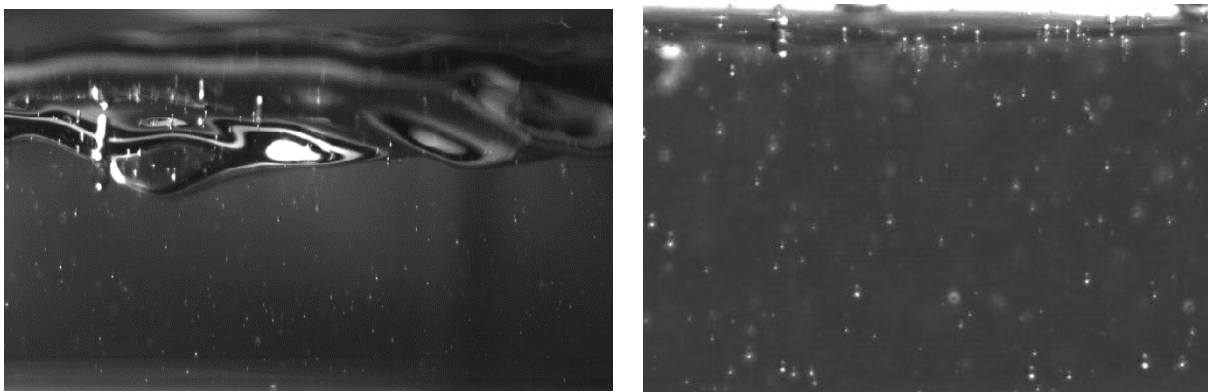


Figure 35 Oxygen bubbles dispersed in water at L/G ratio 0.75, image recorded at point A using pipe B (left), image recorded at point C using pipe A(right)

images recorded at point A for air and water. It was observed that the bubbles produced are well maintained in turbulence as it helps for absorption in the horizontal transparent pipe for a L/G ratio of 1.25. In the Figure 32 (right) as we can see the bubbles are dispersed evenly, the

interfacial area is also good. Whereas in the L/G ratios 1, 0.75 the cylindrical transparent tube is half filled with the oxygen, which makes the horizontal gas-liquid flow regime completely stratified and resultant is poor mass transfer. Another inference from low L/G ratio is that the bubbles coalesce to form much bigger bubbles which sticks to the surface of the transparent tube and not carried by the flow of water. L/G ratio of 1 in higher order ($Q_{air} = 10$ L/min, $Q_{water} = 10$ L/min) is better still in terms of physical observation but the interfacial area is not as good as L/G ratio of 1.25.

In Figure 33, the recorded images of same flow conditions but with different pipe length before the transparent pipe, when pipe B is used for the same L/G ratio the gas – liquid flow regime is sluggish and partly stratified. Also, at point A when using pipe B wavy liquid motion was observed. In this low L/G ratio it is noted that the bubble collision is also high, travels along the liquid motion without being absorbed and escapes out in the gas-liquid separation tank.

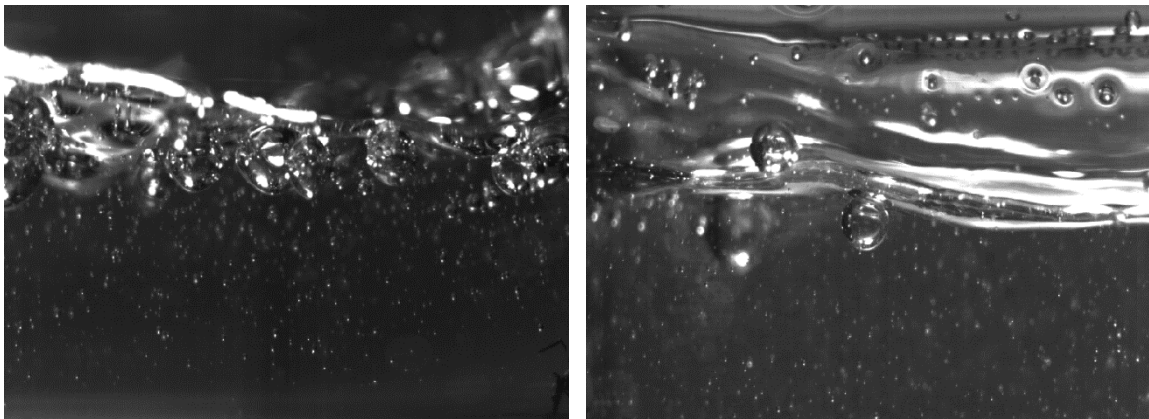


Figure 36 Dissolution of oxygen bubbles, image recorded at point A using pipe A with a L/G ratio of 1.1 (left), image recorded at point C using pipe A with a L/G ratio of 1.25 (right)

In this experiments different L/G ratio were tested, Figure 34 (left) depicts an image of L/G ratio 1 and Figure 34 (right) 1.25, to observe the difference of the microbubble generator turbulence and bubble behaviour. In most of the cases with low L/G ratio, especially when the gas flow is too high than the liquid flow, the gas-liquid flow regime in the horizontal transparent pipe is either sluggish or wavy or even sometimes it is stratified which is not effectively helping the oxygen bubbles to dissolve into water.

9.7.2 8 w-% Na_2CO_3 solution and CO_2

The images of 8 w-% Na_2CO_3 solution and CO_2 was recorded in week #22. It is interesting that for the same flow conditions of air and water the average bubble size is much smaller and rate of coalescence is also low for 8 w-% Na_2CO_3 solution and air.

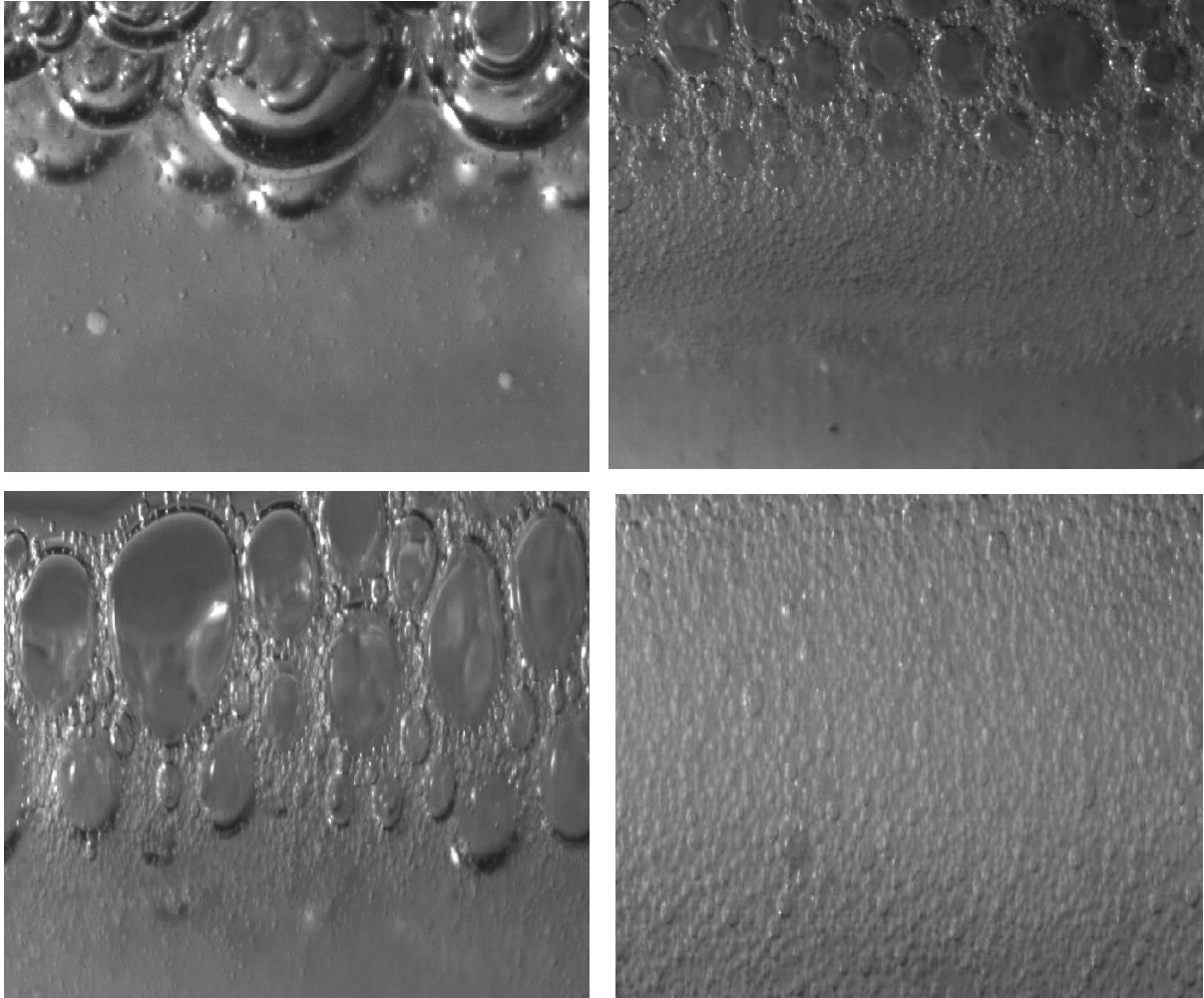


Figure 37 CO_2 bubbles in 8 w-% Na_2CO_3 solution, images recorded at point A using pipe B, L/G ratio 1 (top-left), L/G ratio 1 ($Q_{\text{CO}_2}=10$ L/min, $Q_{8\text{w-\%Na}_2\text{CO}_3}=10$ L/min) (top-right), L/G ratio 0.75 (bottom-left), L/G ratio 1.25 (bottom-right)

It has to be taken into consideration that pipe B is used of which the Figure 35 represents. The idea of having two pipe lengths is to analyse how the delay effects the mass transfer and here to compare physically how the flow and bubbles behave. The observation stands almost similar to air and water for low L/G ratio. It is evident that more finer bubbles are generated when compared to air- water observation even at low L/G ratio. Since pipe B is implemented even at

high L/G ratio after point C the flow gets segregated and bigger bubbles accumulate, since the turbulence from the microbubble generator decreases after point C.

Figure 36 which illustrates the full transparent pipe and images recorded at various points for L/G ratio of 1.25 gives a good idea about the dispersion of the bubbles. It is also to be noted that this image corresponds to the curvature/walls of the transparent tube. Even at this L/G ratio

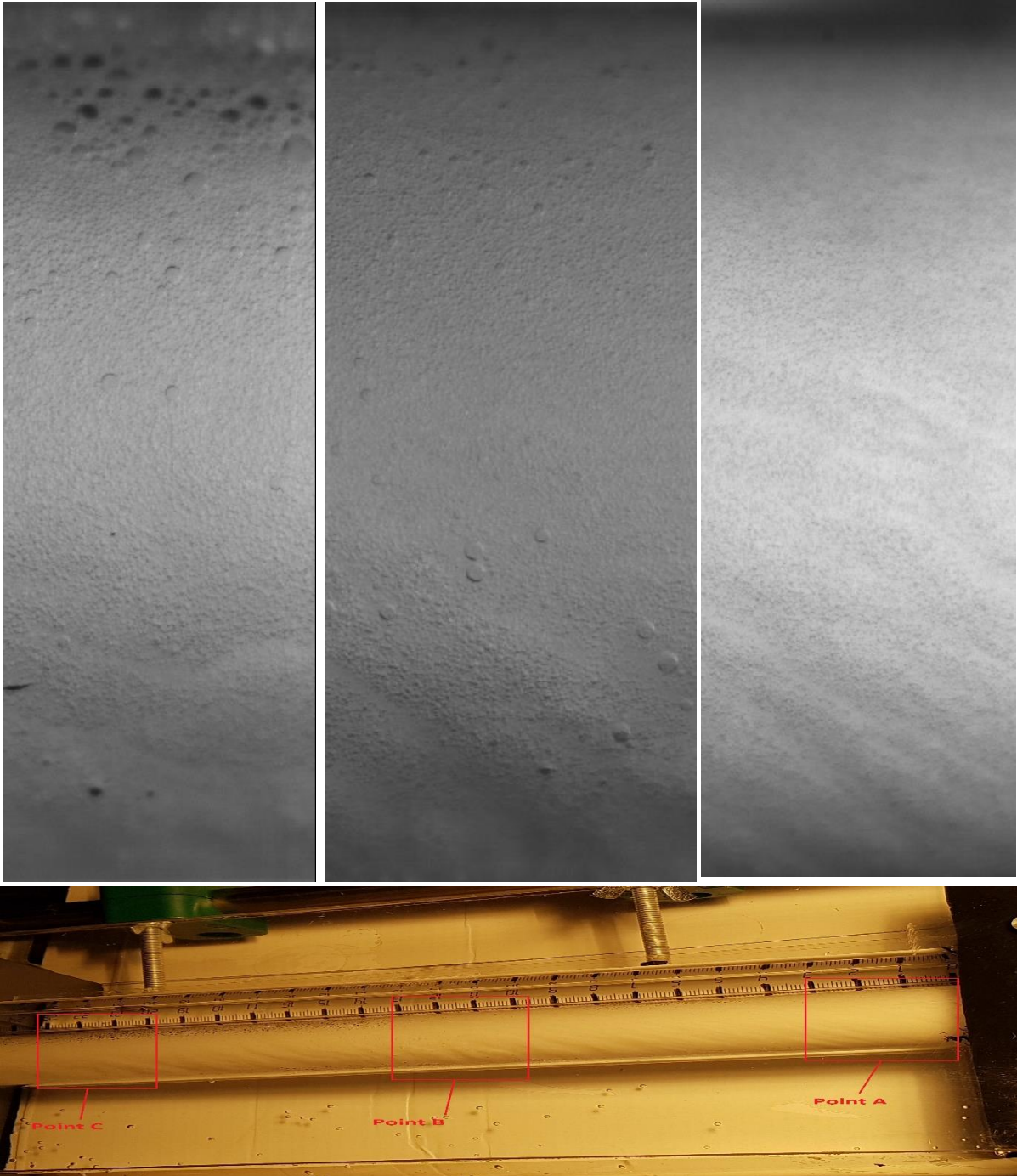


Figure 38 CO₂ bubbles in 8 w-% Na₂CO₃ solution, recorded images for L/G ratio 1.25 using pipe A, image (top-left) represents recorded at point C, image (top-middle) represents recorded at point B, image on the (top right) represents recorded at point A, image at the bottom represents the full transparent pipe of L/G ratio 1.25

of 1.25 some bubbles of slightly bigger in size slowly moves along the walls (especially at the top) while it was observed from the experiments smaller bubbles tend to move faster in-between the bigger bubbles. At L/G ratio the liquid tends to be highly foamy which setbacks the investigation deeper into the liquid from the focal area.

9.7.3 8 w-% Na_2CO_3 solution and CO_2 with vertically mounted microbubble generator

The images of vertically mounted microbubble generator were recorded in week #34. Considerable amount of difference can be observed while the microbubble generator was mounted vertically, especially in L/G ratio of 1 ($Q_{\text{CO}_2}=10$ L/min, $Q_{8\text{w-\%Na}_2\text{CO}_3}=10$ L/min). One primary observation was the axial mixing, because the lower flowrate of liquid does not push all the bubbles enough to pass through the transparent pipe or the liquid flowrate is not enough to beat the gravity since the liquid is heavy, it travels out of the core line and collides with the walls of the transparent pipe carrying the bubbles.

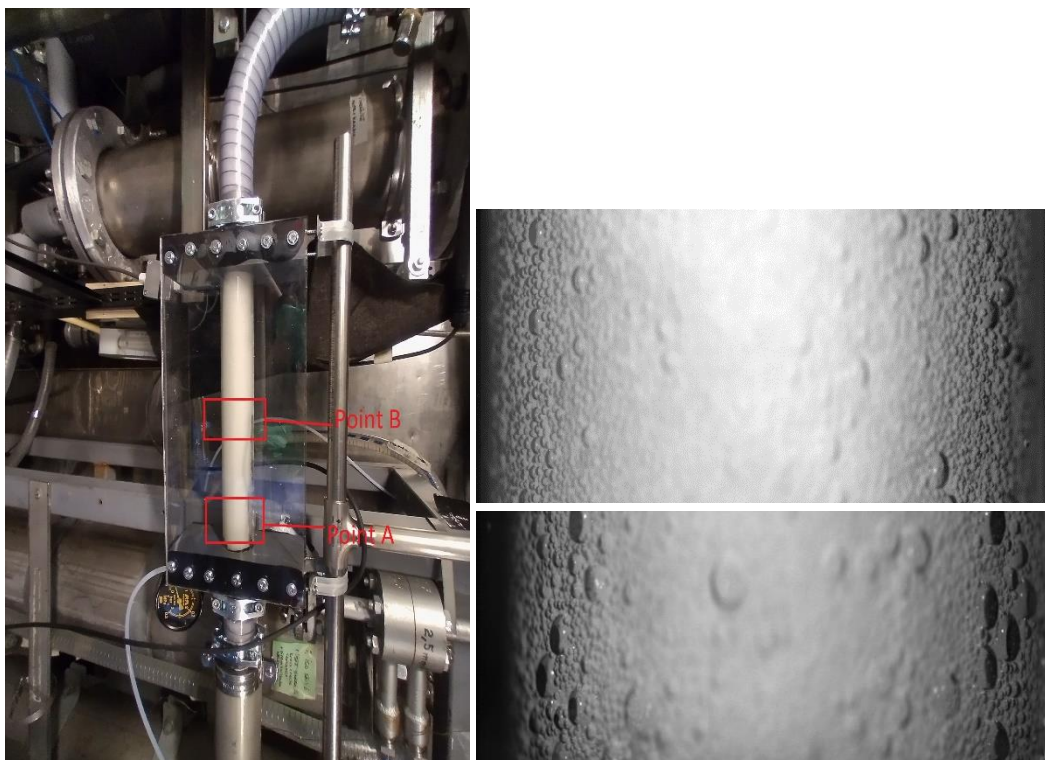


Figure 39 Image of vertically mounted ejector(left), images recorded for L/G ratio 1 at point A(right-bottom), point B (right-top)

By means of physical observation the flow regime would be bubbly-slug transition. In this measurement only pipe A was used and images were recorded only in point A and B.

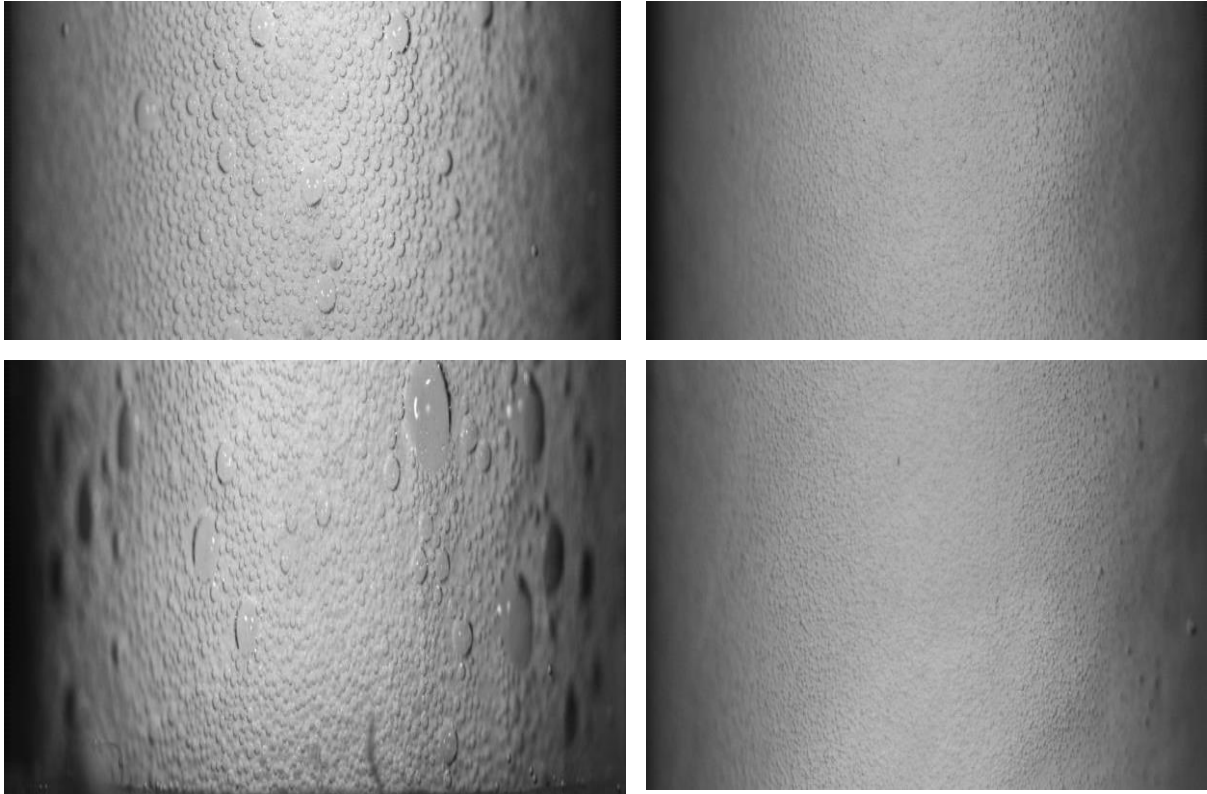


Figure 40 Images recorded for L/G ratio 1(left bottom, top) at point A and B respectively. Images of L/G ratio 1.25 (right bottom, top) at point A and B respectively

Figure 38 compares the L/G ratios of 1 and 1.25, it was observed that at low flowrates bubbles of bigger size appear and sticks to the walls of the pipe, only the core area of liquid carries bubbles out of the transparent pipe, the rate of coalescence in general is low compared to horizontal microbubble generator. Even higher L/G ratio was tested in the experiments which results in higher turbulence and limits the camera to penetrate deep due to intense bubbles around the inner walls of the transparent pipe. In Appendix 1.6 the calculation procedures are explained.

9.7.4 Flow regime comparison for two phase flow in horizontal pipe

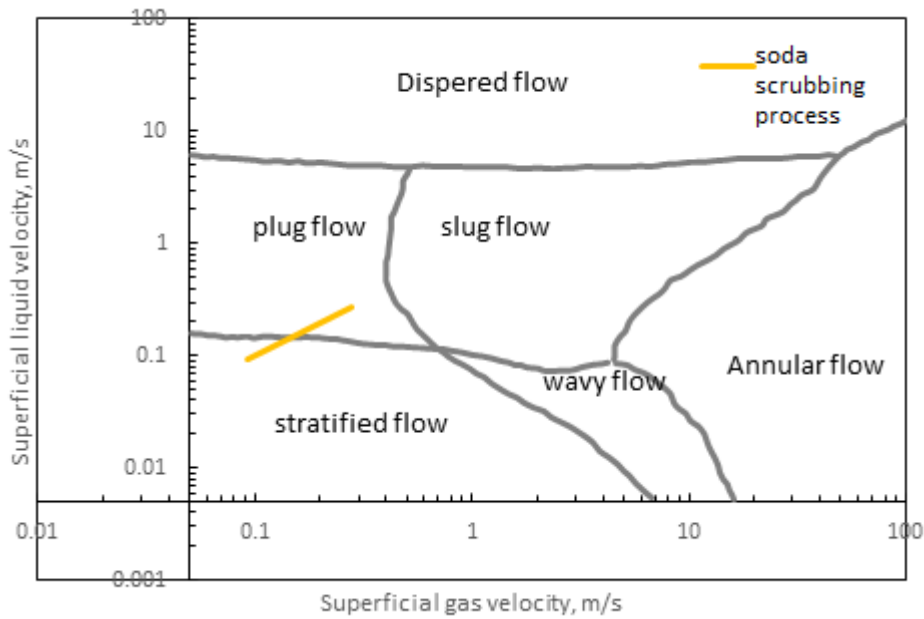


Figure 41 Flow regime map for different gas-liquid in a horizontal pipe (adopted from (Kadri, 2009)) and comparison with experimental values

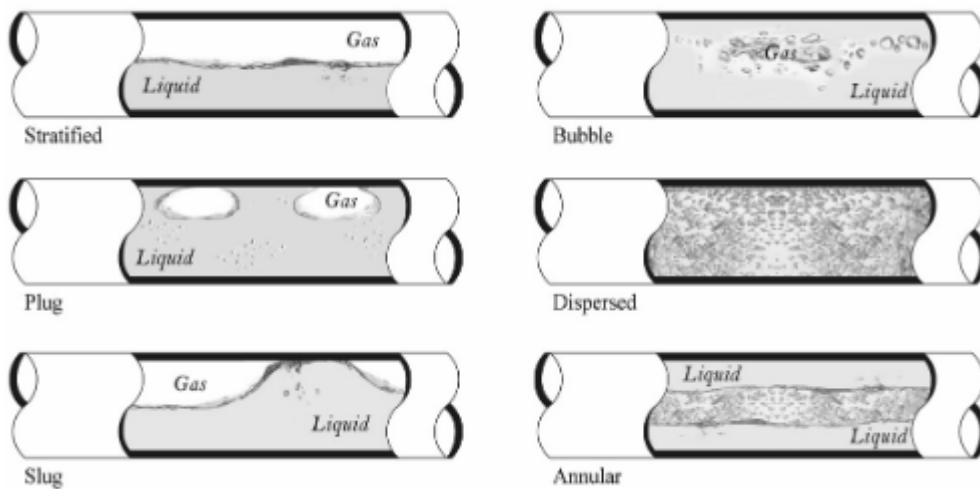


Figure 42 Sketches of flow regimes for gas liquid in a horizontal pipe (adopted from (Kadri, 2009))

Figures 45 and 46 represent flow regimes and flow regime map for gas-liquid in a horizontal pipe. An experiment by Kadri was performed to analyse the reason behind the formation of very long slugs in the pipe. A pipe of 0.054 m diameter was used in Kadri's experiments in which air and water were used and the pipe diameter was similar to the pipe used in our experiments. Due to low gas and liquid pressure and also gravity is perpendicular to the flow direction, gas and liquid exhibit stratified liquid flow at these conditions. Stratified- wavy flow

patterns can be inferred from L/G ratio of 0.75 from our experiments. At higher L/G ratio the flow pattern is observed to be dispersed, due to high intensity of bubbles.

9.8 Pumping energy as a trade-off for $k_L a$

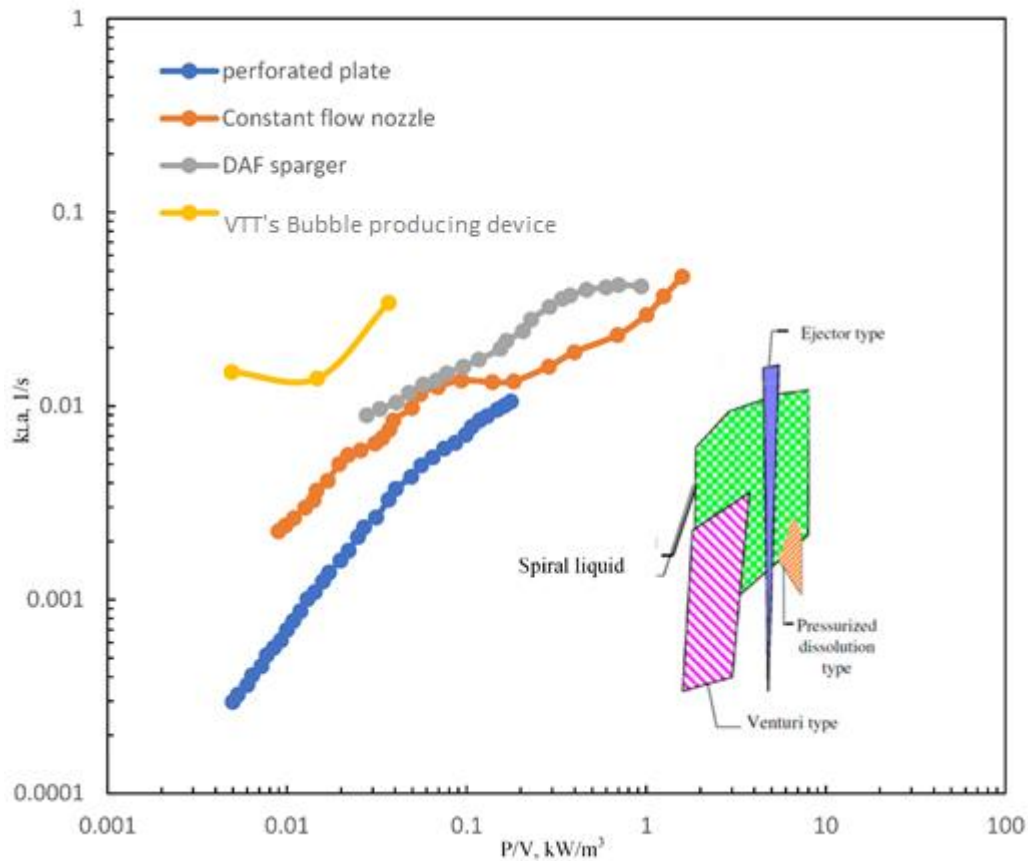


Figure 43 Specific power requirements for various bubble producing devices and comparison with VTT's bubble producing device used in experiments involving air and water (adopted from (Terasaka, 2011))

In figure 47 specific power requirements were compared with different aerators for water and air. The bubble producing device developed by VTT shows promising results at relatively low power consumption, it is already more efficient than other aerators which is compared by Gradov (Dmitry Vladimirovich Gradov., 2020). A detailed calculation procedure is described in Appendix 1.5. Figure 9 and 47 cannot be compared since the bubble producing devices compared in figure 9 are totally higher in power consumption.

10 EVALUATION OF THE EXPERIMENTS AND LIMITATIONS

In this section the effect of different parameters on system efficiency and performance is discussed. It is to be further investigated deeper to get more accurate optimization conditions.

10.1.1 CO₂ capture rates

Most of the post combustion carbon capture technologies are designed with a carbon capture rate of more than 90%, to which VTT's Enhanced soda scrubbing is more efficient. When comparing to the delay pipeline lengths A and B, from Table 4 which compares all the experiments combined but, in this case, comparing within the same pH range would be more logical which is represented in Table 5. To take a deeper look, we also need to consider how much runs are repeated with higher L/G ratio in the same pH range than comparing it with total run time, it is quite experimental that more the times higher L/G is used, higher will be the interfacial area in the gas-liquid flow regime and results in higher capture rate. Also in terms of scaling up this process with lower L/G ratio, without delay length can possibly achieve more better results than using delay length. We also tested the system by maintaining low liquid level in the gas-liquid separation tank to check how efficient the gas-liquid separation tank was. In general mass transfer between surface and liquid inside is very small. When comparing the results in Table 5, the experimental run time and the times of usage of higher L/G ratio is half and same respectively. So mass transfer in gas-liquid separation tank is not intensive and very less which does not help in improving the capture rates.

Testing the system with mounting the microbubble generator in vertical position seems promising, because even with lower flowrates (e.g. $Q_{CO_2}=10$ L/min, $Q_{8w-\%Na_2CO_3}=10$ L/min) the gas-liquid flow regime in vertical transparent pipe is interesting and far better interfacial area is achieved by means of axial mixing. But no strong conclusions can be drawn unless it is tested more extensively. Additionally, to enhance the capture efficiency the simple process in the gas-liquid separation tank should be intensified nevertheless it will increase the capital costs. In a commercial perspective capture rate of about 90% is well in pertinence with industrial scale operations.

10.1.2 Mass transfer rate estimation

The $k_L a$ is influenced by many parameters but then primarily governed by flow conditions, each of the flow combinations would result in a different $k_L a$ value for different parts of the system which is represented by table 12.

The $k_L a$ value is estimated using a model assuming plug flow, by dynamic mass balance from CO_2 in and out.

Table 13 $k_L a$ using pipe A and in gas-liquid separation tank of the VTT's Enhanced soda scrubbing unit

Flow rate(L/min)		$k_L a$ (1/s)	
Q_{CO_2}	$Q_{8\text{w}\text{-}\% \text{Na}_2\text{CO}_3}$ solution	Using pipe A	In gas-liquid separation tank
5	5	0.01	0.001
10	15	0.2	0.001
10	7.5	0.01	0.001
10	10	0.01	0.001
15	15	0.25	0.0015

The base line for the model is the equilibrium concentration in the liquid is dependent on the gas phase partial pressure which changes dynamically when the CO_2 is transferred from gas to liquid even if $k_L a$ remains constant. Practically the advantage of foreseeing the mass transfer rate is that we could choose the concentration of the pollutant gas at the vent for a specific time period provided the flow conditions are estimated. The process of calculating $k_L a$ for different parts of the experimental setup is discussed in Appendix 1.3.

In the MATLAB model of estimating the mass transfer coefficient for oxygen and air, the whole system is assumed to be plug flow, fully mixed model. It is also assumed that there is no mass transfer happening in gas-liquid separation tank. Since the of bubble dispersion degree is unknown which is experimentally characterized, we cannot assume the gas -liquid separation tank to be modelled as plug flow with axial dispersion model nor we could assume it to be a CSTR since we do not know the difference in liquid height when it is aerated and unaerated.

Conclusions from section 9.5.2

1. The reaction is sufficiently fast so that the concentration of CO_2 in the bulk of the liquid phase is close to zero.
2. The reaction rate is such that no appreciable amount of reaction takes place in the diffusion films

An attempt was made to measure the local mass transfer rates for CO₂ and 8 w-% Na₂CO₃ solution by mixing thymol blue and ethanol as an indicator. The expected colour change was from yellow to blue when it reaches a pH of 8.00-9.6, unfortunately the colour change was not observed as expected.

10.1.3 Bubble size measurements

As observed from the experiments the CO₂ gas bubbles in 8 w-% Na₂CO₃ solution tends to stay small and also the rate of coalescence is very low, it is because the ionic layer around the bubbles repels from each other and so once broken or produced tend by the microbubble generator tend to stay small.

Also at lower L/G ratio by using camera we could penetrate a depth of 1.7cm from the walls of the tube to record the images of bubbles. At higher L/G ratio the core of the liquid is not possible to record due to high intensity of the bubbles. While studying the flow dynamics it is instrumental to know how the core area of the liquid behaves for different flow conditions, since the velocity field is also maximum at the centre of liquid. CFD modelling or tomography would give an excellent idea about L/G ratio. The sequence of calculating bubble size and other dimensionless numbers are discussed in Appendix 1.6.

11 CONCLUSION

Improvement in mass transfer efficiency of CO₂ capture using soda solutions has its own advantages and limitations which in this thesis studied in detail. In an overall manner this technology seems much promising having some hidden areas left without in-depth study. The mass transfer efficiency for the system with no reaction (dissolved oxygen measurements) estimated from the MATLAB model is pertinent to other previous research work, comparing the figure 47 (experiment curve) it seems more efficient than other aerators. The $k_L a$ estimated from the CO₂ and 8 w-% Na₂CO₃ experiments with the model in MS excel also looks good in agreement with the estimated values from experiments comparing Figure 6.

The capture rates are interesting, for all the experimental setup the capture rate was almost 90% with reference to Figures 26, 27 and 29 which is much expected but the pressure maintained in the system was 1 bar which is slightly higher in other methods of CO₂ capturing since in this experiments we consider only absorption and not regeneration. Methods which involve regeneration like water scrubbing needs typically 4-6 bar pressure . The CO₂ capture depends on the speed of gas absorption and the residence time of the system. The speed of absorption is dominated by the driving force which is the concentration difference between gas and liquid.

In another view how much of CO₂ can be absorbed at that particular partial pressure of CO₂ in the liquid and how much saturated already the liquid is by CO₂ plays a crucial part. Furthermore, the flow parameters, turbulence, interfacial area will also influence the rate of gas absorption.

The interchangeable pipes i.e., pipe A (10 cm) and pipe B (100cm) was primarily tested how the delay influences the capture rate and the affects the overall system efficiency. It is very evident from the analysis of results of experiments that pipe A is more efficient in terms of capture rate, interfacial area and very less bubble agglomeration is observed. Longer delay time did not had effect on capture rate, so pipe B is less efficient than pipe A.

Residence time is a crucial factor for gas-liquid mass transfer, in this system the performance is highly dependent on residence time which is estimated in table 5. It is found that with a residence time of 5.6 seconds with pipe A gives better performance. The gas-liquid separation tank which has higher number with the residence time does not give good results with capture of CO₂. Longer the residence time increases the bubble agglomeration and mass transfer between the surface and liquid inside is very small even though they are in contact. The over design of gas-liquid separation tank is a limitation to the pilot plant's performance.

From the experiments of CO₂ and 8 w-% Na₂CO₃ solution, aqueous solutions are more effective for CO₂ capture when compared to water since the absorbed CO₂ reacts with alkaline solution, if this the case then the driving force between gas and liquid can be prolonged to a maximum degree as high as with fresh solution containing no absorbed CO₂ because the absorbed CO₂ reacts immediately.

When comparing the different experimental setup used in the experiments, bubble producing device in horizontal position and with pipe A gives best results, rather using pipe B bubbles agglomerate and creates a deficiency in better performance. When the liquid level in gas-liquid separation tank is maintained low, comparing this with pipe A results gives us the result that mass transfer in gas-liquid separation tank is very low and when the bubble producing device is mounted vertically the performance of the system is better and promising still it needs more investigation to draw a conclusion out of it.

The reaction of dissolved CO₂ at the gas liquid interface will make the absorption faster. The magnitude of how much time it is faster is estimated by the enhancement factor. Approximately the absorption rate is 5 to 10 times faster with chemical reaction which depends on the pH and flow conditions. The results also indicates that not only absorption rate but also absorption

capacity is better for soda solutions when compared to water. Nevertheless, the absorption rate significantly depends on the pH and comparing same pH range that has been obtained from the process involving regeneration would be of greater use.

Bubble size varies with respect to the flowrates of gas and liquid. The L/G ratio of 1.25 produces bubbles of smaller size and at liquid Reynolds number of 6790, the interfacial area looks good from physical observation. It is also an inference from the experiments that the $k_L a$ increases to 0.0342 from 0.0167 (1/s) with smaller bubbles.

To conclude, in this thesis work the objectives of determining local mass transfer rates was achieved, needed residence time in CO₂ – sodium carbonate system to reach desired CO₂ capture efficiency was estimated to be 5.6 seconds. Over all mass transfer rate of CO₂ dissolution in enhanced soda scrubbing process using microbubble generator as a function of liquid and gas flow is achieved using the MATLAB model and determined overall mass transfer rate for different gas and liquid flow. The optimal process conditions were determined to be L/G ratio of 1.25 and pumping energy input as a function of mass transfer rate was also established which seems to be very promising for the bubble producing device developed by VTT. An MS Excel model was developed which is used to estimate the performance of the process as function of residence time and flowrate of liquid, gas.

12 FUTURE RESEARCH

The optimal conditions of this experimental setup is deduced in this thesis work still the design of the gas- liquid separation tank can be modified so that there is a low residence time in the gas - liquid separation tank which will further improve the efficiency. Also vertically mounted bubble producing device shows promising results which needs to be investigated further.

13 REFERENCES

- Agency, I. E., 2019. *Putting CO₂ to Use: creating value from emissions*, Paris: IEA.
- Ajay Mandal, G. k. D. M., 2003. Interfacial Area and liquid side volumetric mass transfer coefficient in adownflow bubble column. *The Canadian Journal of Chemical Engineering*, Volume 81, pp. 212-219.
- Ausfelder, F. and Wagemann, K., 2020. Power -to-fuels:E-fuel as an important option for a climate -friendly mobility of the future. *Chemie ingenieur technik*, Volume 92, pp. 21-30.
- Barbara.P, S., 2009. Greenhouse gas mitigation in a carbon constrained world: The role of carbon capture and storage. *Energy Policy*, 37(12), pp. 5081-5093.
- Bedekar, S. C., 1995. Properties of sodium carbonate-sodium bicarbonate. *applied chemistry*.
- Branan, C. R., 1999. *Pocket Guide to Chemical Engineering*. s.l.:Elsevier Science and Technology Books.
- Brett P, S., 2013. *A novel Approach to Carbon Dioxide Capture and Storage*, Michigan: Michigan Technological University.
- C.R Harte, J., Baker, E. and Purcell, H., 1933. Absorption of CO₂ in sodium Carbonate - bicarbonate solutions. *Industrial and Engineering Chemistry*, 25(5).
- Cai, Y. et al., 2018. Effective Capture of Carbon Dioxide Using HydratedSodium Carbonate Powders. *MDPI materials*, 24 January.
- Chang HunLee, H. D.-W. D. E. S. W. H. S., 2019. Experimental investigation of microbubble generation in the venturi nozzle. *International Journal of Heat and Mass Transfer*, Volume 136, pp. 1127-1138.
- Coulson, J. et al., 1999. *Chemical Engineering Volume 1- Fluid flow, Heat Transfer and Mass transfer*. s.l.:Elsevier.
- Cui, S., Borgemenke, J., Liu, Z. and Li, Y., 2019. Recent advances of “soft” biopoly carbonate plastics from carbon dioxide and renewable bio-feedstocks via straightforward and innovative routes. *Journal of CO₂ Utilization*, Volume 34, pp. 40-52.
- cyclopedia, C. M., 2015. *Multiphysics cyclopedia*. [Online]
Available at: <https://www.comsol.com/multiphysics/what-is-mass-transfer>
- Davide pinelli, Z. L. F. M., 2010. Analysis of K_{La} measurement methods in stirred vessels: The role of experimental techniques and fluid dynamic models. *International Journal of chemical reactor engineering*, Volume 8.
- Dmitry Vladimirovich Gradov., e., 2020. Auto-Aspirated DAF Sparger Study on Flow Hydrodynamics, Bubble Generation and Aeration Efficiency. *Process* , 8(1498).
- Emerson, S. and Hedges, J., 2008. *Chemical Oceanography and the marine carbon cycle*. Cambridge: Cambridge University press.

Fernández-Dacosta, C. et al., 2017. Prospective techno-economic and environmental assessment of carbon capture at a refinery and CO₂ utilisation in polyol synthesis. *Journal of CO₂ Utilization*, Volume 21, pp. 405-422.

Figuerola, J. D. et al., 2008. Advances in CO₂ capture technology—The U.S. Department of Energy's Carbon Sequestration Program. *International Journal of Greenhouse Gas Control*, 2(1), pp. 9-20.

Ganan-Calvo, A. M. and Gordillo, J. M., 2001. Perfectly Monodisperse Microbubbling by Capillary Flow Focussing. *Physical Review Letters*, 87(27).

Gradov, D. V., 2020. Auto-Aspirated DAF Sparger Study on Flow Hydrodynamics, Bubble Generation and Aeration Efficiency. *MDPI*, 8(11).

Green, D. A. et al., 2004. Carbon dioxide capture from flue gas using dry regenerable sorbents, Pittsburgh: U.S. Department of Energy National Energy Technology laboratory.

Hannula, I. and Melin, K., 2021. Biorefineries with CCS, Cheltenham: IEAGHG Technical report.

Hermann, C., Dewes, I. and Schumpe, A., 1995. The estimation of gas solubilities in salt solution. *Chemical Engineering Science*, 50(10), pp. 1673-1675.

Hessen, T. E. et al., 2010. Vapor–liquid equilibrium in the sodium carbonate–sodium bicarbonate–water–CO₂-system. *Chemical Engineering Science*, 65(6), pp. 2218-2226.

Hikita, H., Asai, S. and Takatsuka, T., 1976. Absorption of Carbon Dioxide into Aqueous Sodium Hydroxide and Sodium Carbonate-Bicarbonate Solutions. *The Chemical Engineering Journal*, Volume 11, pp. 131-141.

Hosten, L., 1984. Kinetics of gas-liquid reactions. *Periodica Polytechnica Chemical Engineering*, 28(1), p. 19–39.

Huang, J. et al., 2020. An investigation on the performance of a micro-scale Venturi bubblegenerator. *Chemical engineering journal*.

Huttenhuis, P., Roeloffzen, A. and Versteeg, G., 2016. CO₂ Capture and Re-use at a waster Incinerator. *Energy Procedia*, pp. 47-55.

International, B., 2019. Bio energy International. [Online] Available at: <https://bioenergyinternational.com/heat-power/stockholm-exergi-to-test-carbon-capture-at-vartan-biomass-chp-plant>

Jose M, G., Cheng, Z., Calvo, A. M. G.-. and Marquez, M., 2004. A New device for the generation of Microbubbles. *Physics of Fluids*, 16(8).

Kadri, U., 2009. Long liquid slugs in stratified gas/liquid flow in horizontal and slightly inclined pipes, Amsterdam: Delft University.

Knuutila, H., Juliussenb, O. and Svendsen, H. F., 2010. Density and N₂O solubility of sodium and potassium carbonate solutions in the temperature range 25 to 80 C. *Chemical engineering science*, Volume 65, pp. 2177-2182.

- Knuutila, H., Juliussenb, O. and Svendsen, H. F., 2010. Kinetics of the reaction of carbon dioxide with aqueous sodium and potassium carbonate solutions. *Chemical Engineering Science*, Volume 65, pp. 6077-6088.
- Knuutila, H., Svendsena, H. F. and Juliussen, O., 2009. Kinetics of carbonate based CO₂ capture systems. *Energy Procedia*, pp. 1011-1018.
- Levihn, F., Linde, L., Gustafsson, K. and Erik Dahlen., 2019. Introducing BECCS through HPC to the research agenda: The case of combined heat and power in stockholm.. *Energy Reports*, Volume 5, pp. 1381-1389.
- Liew, K. C. S., rasdi, A. and et.al, W. B., 2020. Porous Venturi-Orifice Microbubble Generator for Oxygen Dissolution in Water. *Processes*, Volume 8.
- Lu, Y. et al., 2011. Development of a Carbonate Absorption-Based Process for Post-Combustion CO₂ Capture: the Role of Biocatalyst to Promote CO₂ Absorption Rate. *Energy Procedia*, pp. 1286-1293.
- Ma'mun, S., Dindore, V. Y. and Svendsen, H. F., 2007. Kinetics of the Reaction of Carbon Dioxide with Aqueous Solutions of 2-((2-Aminoethyl)amino)ethanol. *Industrial Engineering Chemistry*, Volume 46, pp. 385-394.
- Mandal, A., Kundu, G. and Mukherjee, D., 2003. Interfacial Area and Liquid-Side Volumetric Mass. *Canadian Journal of Chemical Engineering*, Volume 81, pp. 212-218.
- McCabe, W. L., Smith, J. and Harriot, P., 1993. *Unit operations of chemical engineering*. s.l.:McGraw-hill International.
- McCoy, H. N. and Herbert J. Smith, 1911. Equilibrium Between Alkali- earth Carbonates, carbon dioxide and water. *General, Physical and Inorganic*, pp. 468-473.
- Morsi, B. I. and Basha, O. M., 2015. Mass Transfer in Multiphase Systems, Mass Transfer - Advancement in Process Modelling. In: *Mass Transfer-Advancement in process Modelling*. s.l.:IntechOpen.
- Nevander, M., 2021. Process modelling and techno-economic evaluation of production of CO₂ based polycarbonate polyols. Espoo: Aalto University.
- Perry, R. H. and Green, D. W., 1997. Heat and Mass Transfer. In: *Perry's Chemical Engineer's Handbook*, Seventh edition. s.l.:McGraw Hill.
- Qingdao Echemi Technology Co., L., 2018. echemi.com. [Online] Available at: <https://www.echemi.com/productsInformation/pd20150901033-sodium-bicarbonate.html>
- Roberts, D., 2019. Pulling CO₂ out of the air and using it could be a trillion-dollar business. [Online] Available at: <https://www.vox.com/energy-and-environment/2019/9/4/20829431/climate-change-carbon-capture-utilization-sequestration-ccu-ccs>
- Rodrigo A, G., Janusz S, . L. and Heiskanen, , K., 2005. Effect of frother on bubble size. *International journal of mineral processing* , 76(4), pp. 225-223.

- Schneider, T., 2019. Last Exit E-fuels. *MTZ Worldw* 80, pp. 16-19.
- Shim, J.-G., Lee, D. W., Lee, J. H. and Kwak, N.-S., 2016. Experimental study on capture of carbon dioxide and production of sodium bicarbonate from sodium hydroxide. *Environmental Engineering Research*, Volume 21, pp. 297-303.
- Shrestha, P., 2020. carbon footprint comparison between traditional diesel and synthetic diesel production pathways, Lappeenranta: Lappeenranta–Lahti university of technology.
- Sipila, J. T. Z., 2007. Carbon dioxide sequestration by mineral carbonation, Turku: Abo Akademi University.
- Spigarelli, B. P., 2013. A Novel Approach to Carbon Dioxide Capture and Storage, Michigan: Michigan Technological university.
- Stefan Siegemund, d., 2017. The potential of electricity- based fuels for low-emission transport in the EU, Berlin: German Energy Agency.
- Terasaka, K. e. a., 2011. Development of microbubble aerator for waste water treatment using aerobic activated sludge. *Chemical Engineering Science*, Volume 66, pp. 3172-3179.
- Tervasmäki, P., 2018. Reaction and mass transfer kinetics in multiphase bioreactors. Oulu, Finland: University of Oulu.
- Tracker, C. A., 2019. Governments still showing little sign of acting on climate crisi. [Online] Available at: <https://climateactiontracker.org/publications/governments-still-not-acting-on-climate-crisis/> [Accessed 2019].
- Treybal, R. ..., 1981. Mass-Transfer Operations. s.l.:McGraw-Hill Chemical Engineering Series.
- UNEP, 2019. UNEP. [Online].
- Wanga, M. et al., 2011. Post-combustion CO₂ capture with chemical absorption: A state-of-the-art review. *Chemical engineering research and design*, Volume 89, pp. 1609-1624.
- Wang, K., Xia, L., Lu, Y. and Luo, G., 2013. Generting microbubbles in a co-flowing microfluidic device. *Chemical Engineering Science*, Volume 100, pp. 486-495.
- Vasconcelos, Orvalho, J. M. T., P, S. and Sebastiao S, A., 2002. Gas-liquid mass transfer to single bubbles: Effect of surface contamination. *Americal Institute of Chemical Engineers*, 48(6), pp. 1145-1154.
- Vázquez, G. et al., 2000. Application of the Danckwerts method in a bubble column: Effects of surfactants on mass transfer coefficient and interfacial area. *Chemical Engineering Journal*, 78(1), pp. 13-19.
- Weisenberger, S. and Schumpe, A., 1996. Estimation of gas solubilities in salt solutions at temperatures fro 273K to 363 K. *AICHE Journal*, 42(01), pp. 298-300.
- Vericella, J. J. et al., 2015. Encapsulated liquid sorbents for carbon dioxide. *Nature Communications*, Volume 6.

Vinca, A., Rottoli, M., Marangoni, G. and Tavoni, M., 2018. The role of carbon capture and storage electricity in attaining 1.5 and 2 °C. *International Journal of Greenhouse Gas Control*, Volume 78, pp. 148-159.

VTT, 2021. VTT, Neste and their partners seek breakthrough in Finnish e-fuel technology. [Online]

Available at: <https://www.vttresearch.com/en/news-and-ideas/vtt-neste-and-their-partners-look-for-breakthrough-in-finnish-e-fuel-technology>

[Accessed 08 02 21].

YSI, 2020. YSi, a xylem Brand. [Online]

Available at: <https://www.ysi.com/proodo>

YSI, 2021. YSI, a xylem brand. [Online]

Available at: <https://www.ysi.com/customer-support/software-firmware-downloads/software>

Appendix

Calculation algorithm is described sequentially in this part.

Appendix 1.1 : Modelling in MATLAB

Primary task of this model is to establish the $k_L a$ values for air and water, CO_2 and 8w-% Na_2CO_3 solution. In this model we use nonlinear least squares method to minimize the deviation to the smallest possible, i.e., minimizing the sum of the squares of the residual errors. The ODE equations were solved, and all the variables are data fitted for $k_L a$.

The block diagram below which represents the sequence of how the optimized $k_L a$ is been obtained.

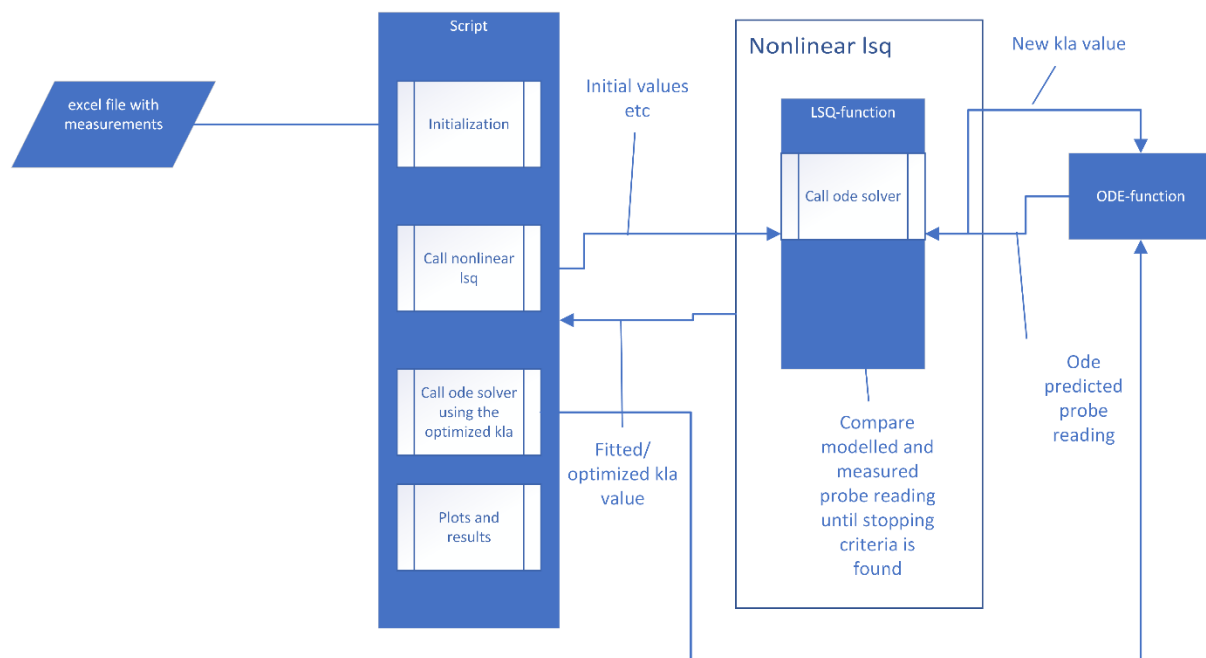


Figure 44 Sequence of the MATLAB Model

Basically, in the script file we have the excel input which contains time, dissolved oxygen concentration and corresponding temperature from the experiments. The initialization and the input values for other variables are provided in the script. The initial values are fed to the nonlinear least square function. The nonlinear least square function stops until or continues to work until it minimizes the residual parameter, for which the input is also obtained from the ODE function which solves the ODE equations and finds a new $k_L a$ value for each iteration. Essentially the model is solved with the $k_L a$ as a free parameter to data fit the dynamics of the

measured DO readings from the experiments to the probe readings taking response time into account.

In the data fitted plot we have 3 curves (which is shown below),

1. DO measured from the experiments- which contains the time lag.
2. DO probe – which is the corrected DO readings that includes the time lag
3. DO data fitted- which is the model fitted to the DO probe by generating the new $k_L a$ value for each iteration.

ODE equations

The genesis of the ODE equations originates from the mass balances which is generally described as oxygen transfer rate.

PFR Modelling

Conditions: Unsteady state, fully mixed model – Dynamic, Plug flow reactor

Mass Balance:

$$\text{Inlet} + \text{Generation} = \text{Outlet} + \text{Consumption} + \text{Accumulation} \quad (32)$$

In case of interfacial mass transfer the Equation (32)

$$\text{Accumulation} = \text{Inlet} - \text{Outlet} + \text{Generation (rate of interfacial mass transfer)} \quad (33)$$

General:

$$\frac{d}{dt} (VC) = (C_i Q_0) - (C_f Q_1) + Q \quad (34)$$

$$\frac{d}{dt} (VC) = (C_i Q_0) - (C_f Q_1) + k_L a (C_{11} - C_{12}) \quad (35)$$

Component specific model equations

For liquid side:

Accumulation = Inlet-Outlet+ Generation (rate of interfacial mass transfer)

when the same liquid is circulated or no input change, Inlet =0, also when the C_L varies with distance, also the O_2 is transferred from gas to liquid, so

$$\frac{d}{dt} (C_L V_L) = C_L Q_L + k_L a (C_g - C_L) \quad (36)$$

$$\frac{d}{dt} C_L = \frac{d}{dx} C_L \frac{Q_L}{V_L} + \frac{k_L a (C_g - C_L)}{V_L} \quad (37)$$

$$\frac{d}{dt} C_L = \frac{Q_L}{(1 - \varepsilon_g) S} \frac{d}{dx} C_L + \frac{k_L a (C_g - C_L)}{(1 - \varepsilon_g) S} \quad (38)$$

The volume of liquid is constant but the volume of gas is not constant there was a negligible change but we assume it to be constant.

In the same way for gas side:

Here the O_2 is transferred from gas to liquid and the gas concentration changes over distance, so

$$\frac{d}{dt} (C_g V_g) = C_g Q_g + k_L a (C_g - C_L) \quad (39)$$

$$\frac{d}{dt} C_g = \frac{Q_g}{\varepsilon_g S} \frac{d}{dx} C_g - \frac{k_L a (C_g - C_L)}{\varepsilon_g S} \quad (40)$$

So there is both transfer of liquid and mass transfer between phases over time and distance happens, consider the equation (38) which is

$$\frac{d}{dt} C_L = \frac{Q_L}{(1 - \varepsilon_g) S} \frac{d}{dx} C_L + \frac{k_L a (C_g - C_L)}{(1 - \varepsilon_g) S} \quad (38)$$

The above equation can be split into two parts

$\frac{Q_L}{(1 - \varepsilon_g) S} \frac{d}{dx} C_L$ - This part explains the movement between the discretized elements of the reactor.

$\frac{k_L a (C_g - C_L)}{(1 - \varepsilon_g) S}$ - This part explains the mass transfer between phases in the system.

Spatial Discretization

Spatial discretization (1D), n is user defined which is tuned until the $k_L a$ value does not change anymore. In this model the length of the Continuous loop reactor (CLR) is estimated by the

total volume. Essentially the CLR is assumed to be a plug flow reactor described in mathematical equations (33) and (34). Specifically, the lengths are obtained from volume equivalents of the pipes and vessels used, to a pipe of average diameter 2.6 cm, then it is split into user defined number of spatial elements. (Gradov, 2020).

The spatial discretization degree has a limitation towards the variation of flowrates. In our experiments the variation of flowrates for gas and liquid range is wide so each flow conditions has its own optimum discretization degree, so that it gives good fit.

From this part $k_L a$ is obtained with no reaction present in the system.

CO₂ Capture rate

The CO₂ capture rates were estimated from mass balances of synthetic gas mixture coming in and leaving the system. The physical and chemical properties of CO₂ rich incoming gas and CO₂ lean gas out was utilized for mass balances as described in equation (39) assuming that N₂ in the incoming synthetic gas mixture leaves out completely.

$$CR(\%) = \frac{y(CO_2)_{in} \dot{v}_{in} - y(CO_2)_{out} \dot{v}_{out}}{y(CO_2)_{in} \dot{v}_{in}} \quad (39)$$

Appendix 1.2 : Mass transfer rate estimation from CO₂ and 8 w-% Na₂CO₃ experiments- Using MS Excel model

Assumptions:

The reaction is sufficiently fast so that the concentration of CO₂ in the bulk of the liquid phase is close to zero.

To justify this assumption the below condition is checked from the recorded experimental values of pH and known parameters

$$k_L a \ll \alpha_L K_2 C_B^0 \quad (30)$$

$$\left[\frac{D_A K_2 C_B^0}{k_L^2} \right] \ll 1 \quad (31)$$

Concentration of $[OH^-]$:

$$pH = -\log_{10}[H^+(aq)] \quad (39)$$

$[H^+(\text{aq})] = 10^{-pH}$, we will get the H^+ ions concentration.

we know that from the basics,

$$[H^+(\text{aq})] [OH^-(\text{aq})] = 1 \times 10^{-14} \text{ (mol/L)} \quad (40)$$

$[OH^-(\text{aq})] = \frac{1 \times 10^{-14}}{[H^+(\text{aq})]}$ (mol/L), we will get the concentration of OH^-

Concentration of CO_3^{2-} (carbonate ion) and HCO_3^- (Bicarbonate ion)

Base dissociation constant for CO_3^{2-} ion, $K_b = 4.2 \times 10^{-7}$,

Base dissociation constant for HCO_3^- ion, $K_b = 4.7 \times 10^{-11}$,

we know that

$$PK_b = -\log [K_b] \quad (41)$$

also

$$pH = PK_b + \log \frac{[OH^-(\text{aq})]}{[CO_3^{2-}]} \quad (42)$$

solving

$$pH - PK_b = \log \frac{[OH^-(\text{aq})]}{[CO_3^{2-}]}$$

$$10^{(pH - PK_b)} = \frac{[OH^-(\text{aq})]}{[CO_3^{2-}]}$$

$$CO_3^{2-} = \frac{[OH^-(\text{aq})]}{10^{(pH - PK_b)}}$$

we know concentration of $[OH^-(\text{aq})]$ from the corresponding pH.

Similarly, for $HCO_3^- = \frac{[OH^-(\text{aq})]}{10^{(pH - PK_b)}}$

$$k_L = 4.5 \times 10^{-3} \times v_{sg}^{0.08} \times \eta_{eff}^{-0.32} \quad (43)$$

$$\alpha = 0.38 \times 10^4 \times v_{sg} \quad (44)$$

$$\log_{10} k_2 = 16.635 - \frac{2895}{T} + 0.132 I \quad (45)$$

$$C_B^o = \frac{K_W}{K_2} \times \frac{[CO_3^{2-}]}{[HCO_3^-]}$$

$$\log K_2 = -2902.4/T + 6.498 - 0.0238 \times T \quad (46)$$

Where ionic strength is concentration of carbonate + concentration of bicarbonate ions.

k_L - liquid side mass transfer coefficient, (cm/s)

α - specific interfacial area, (m^2/m^3)

C_B^o – concentration of reactant B in the bulk of the solution, (mol/L)

k_2 – second order reaction rate constant, (mL/ mol.s)

K_2 – equilibrium values, (mol/L)

I – ionic strength (g ion/L)

D_A – diffusivity of dissolved gas, (cm^2/s)

T- Temperature (K)

v_{sg} – superficial gas velocity, (m/s)

η_{eff} - effective viscosity, (Pa.s)

α_L – fractional liquid holdup

The second condition was also checked and the resultant value is greater than 1, which means appreciable amount of reaction is happening in the liquid films. Both of the conditions is valid for all the pH range the experiments were conducted.

In the excel model the time step value is assumed and initially the $k_L\alpha$ was also assumed. We know from experiments the synthetic gas composition of inlet gas stream (15% CO₂ and 85% N₂), inlet mole fraction is 0.15 for time step 0.

We know that partial pressure is total pressure multiplied by mole fraction

Also we know that equilibrium concentration of CO₂ equals to partial pressure divided by Henry's law constant

Henry's law constant used was $H = 9000 \text{ kPa m}^3/\text{kmol}$ (in 8 w- % Na₂CO₃)

As the condition (30) above was true concentration of CO₂ in the bulk of the liquid phase is assumed to be zero

Flux is calculated as $N = k_L\alpha$ (equilibrium concentration of CO₂ - CO₂ in the bulk of the liquid phase), flux is obtained in mol/s

So now we know that the amount of CO₂ from the flux will go into the liquid in corresponding time step.

So this amount of CO₂ which goes into the liquid will be subtracted from the gas inlet flow (corresponding composition) to know how much of CO₂ is remaining in the gas phase.

Now to calculate the corresponding residence time according to the flowrates and dimensions.

Residence time equals to volume of the equipment divided by flowrate, residence time is obtained in seconds.

So now from the experiments we record the outlet gas composition. We know from recorded values mole fraction of CO₂ for particular time, particular flowrate.

In the deviation column subtract the inlet mole fraction of CO₂ with the outlet mole fraction of CO₂ recorded from the experiments, now we know the residence time for the pipe after the bubble producing device until it reaches the separation tank. We can minimize this deviation using ‘goal seek’ or using solver options in excel file which changes the $k_L a$ value and from here we could obtain the $k_L a$ value for different flowrates.

Appendix 1.3: To get the $k_L a$ for different parts of the system

First the $k_L a$ for the pipe after the microbubble device is obtained based on the values of gas outlet mole fraction recorded from low-liquid level in gas-liquid separation tank.

Assuming that the CO₂ content after the microbubble device and before the vapor liquid separation tank in the experiment with pipe A is same as such in experiment with low liquid level, the $k_L a$ value for the gas- liquid separation tank is obtained from the outlet mole fraction of CO₂ and the CO₂ content of the gas phase before the gas-liquid separation tank.

Appendix 1.4: Enhancement Factor

Enhancement factor is calculated by comparing the values of mass transfer rate calculated from the excel model (with reaction) and values of mass transfer rate obtained from the MATLAB model (without chemical reaction) for corresponding flowrates.

Appendix 1.5: Inlet power and $k_L a$

Pump inlet power is calculated by the equation ()

$$P = \frac{Q\rho gh(P_2 - P_1)}{36 \times 10^5} \quad (47)$$

where P - power, kW, Q - flowrate of liquid, m³/h, g - gravity, m/s², h = differential head, m, P_1 , P_2 are the pressure before and after the bubble producing device.

V is the volume of liquid in the system, m³

Appendix 1.6: Bubble size measurements

Bubble size were measured using PFV software by analyzing 20 bubbles of minimum and maximum size which could be found in the moving stream of liquid. Only bubbles which were in the moving stream of liquid were considered in measurement of bubble diameter. Local bubble flow velocities were also determined by following individual bubbles over a stipulated number of frames. The distance travelled will be measured by the distance measurement scale.

$$\text{Local bubble velocity} = \frac{\text{Distance travelled by the bubble}}{\left(\frac{\text{First frame of the bubble} - \text{last frame of the bubble}}{\text{Frames per second}}\right)}$$

Reynolds number was calculated by,

$$R_{eL} = \frac{\rho_L V_L D}{\mu_L} \quad (48)$$

where V_L – liquid velocity (m/s), D – pipe diameter (m), μ_L – liquid viscosity (Pa s), ρ_L - liquid density (kg/m^3).

Schmidt number was estimated using the below mentioned relationship

Schmidt Number,

$$Sc = \frac{\mu_L}{\rho_L D_c} \quad (49)$$

Sherwood number was also estimated using the below mentioned correlation

Sherwood number,

$$Sh = 0.0818 R_{eL}^{0.872} Sc^{0.5} \quad (50)$$

Liquid phase mass transfer coefficient was established using the below mentioned correlation.

Sherwood number,

$$Sh = \frac{K_L d}{D_c} \quad (51)$$

Since the diameter of the bubble influences the K_L established would give us a rough idea.

μ_L – liquid viscosity (Pa s)

D_c = Diffusion Coefficient (m^2/s) (for CO_2 in water = 1.71×10^{-9} , for CO_2 in 8 wt.% Na_2CO_3 = 1.66×10^{-9} , for oxygen in water = 1.97×10^{-9})

K_L = liquid phase mass transfer coefficient (m/s)

Q – flowrate of liquid/gas (l/s)

A – cross sectional area of the pipe (m^2)

R – radius of the pipe (m)